AN INVERSE MODEL FOR ESTIMATING ELASTICITY OF THE ARTERIAL WALL USING IMMERSED BOUNDARY METHOD

AN INVERSE MODEL FOR ESTIMATING ELASTICITY OF THE ARTERIAL WALL USING IMMERSED BOUNDARY METHOD

By

TUSHAR GADKARI, B.E. (MUMBAI UNIVERSITY)

A Thesis

Submitted to the School of Graduate Studies

In Partial Fulfillment of the Requirements

For the Degree

Masters of Applied Science in Engineering

McMaster University

MASTERS OF APPLIED SCIENCE (2007) **McMASTER UNIVERSITY**

(Electrical and Computer Engineering) Hamilton, Ontario, Canada

TITLE: An Inverse Model for Estimating Elasticity of the Arterial Wall using Immersed Boundary Method.

AUTHOR: Tushar Gadkari.

SUPERVISOR: Dr. Aleksander Jeremic.

NUMBER OF PAGES: xii, 83

ABSTRACT

Atherosclerosis generally occurs near the branching in the arteries where there tends to be flow irregularities. A build up of fatty deposits (plaque) occurs in the blood vessel in such regions making it to lose its elasticity. Such hardening of the arteries and the narrowing of the lumen can cause severe atheromas and even high blood pressure and blockage of the vessels. It is observed in North America that nearly 47% of the deaths are caused due to cardiovascular diseases and hence determination of such regions becomes very critical and can be very beneficial if done at an earlier stage. In this thesis, we present: an approach to model the pulsating flow of blood through such an atherosclerosis affected region of the artery using finite element method and further discuss the statistical model used to implement the optimization techniques to estimate the region of maximum rigidity. Here within we present a numerical and non-invasive approach to predict such regions. The computational modeling is carried out under two categories: a. The mathematical model and b. The statistical model.

The mathematical model which is the forward model, comprises of the artery and the cardiac muscle as hyperelastic material modeled with the neo-hookean model and the three dimensional Navier-Stokes equations solve for the blood flowing through it. We perform fluid dynamic analysis for the blood flowing through the vessel to compute the velocity at different time instances and mechanical analysis to compute the deformation of the artery which is a function of the elasticity of the vessel. The two models are interconnected to each other by boundary conditions as the normal component of the

surface force provides the coupling between the two models. The shear modulus represents a measure of the elasticity of the vessel. We use linear spatial basis functions to model the shear modulus which spatially varies along the geometry of the vessel thus we have a region of atherosclerosis and the geometry shows the stenosis. The change in the shear modulus affects the velocity of blood through the vessel.

In the statistical model, we propose an inverse computational model for estimating the elasticity profile of the arterial wall where we implement the inverse modeling approach to estimate the maximum shear modulus which helps us to predict the region of atherosclerosis. The velocity and the deformation obtained for a particular shear modulus from our *COMSOL* forward model provide the realistic simulated measurements that are made noisy by introduction of white Gaussian noise with different *SNR* and we try to estimate the shear modulus that minimizes the error-function. We use *COMSOL* with *MATLAB* for simultaneous iterative computations of velocity and deformation measurements by running the optimization code. We estimate these unknown parameters using optimization algorithm that minimizes the cost function of our model. For our estimation we use the least squares estimator and we derive the maximum likelihood estimator. The unconstrained optimization is carried out with Nelder Mead Simplex Method and the Trust Region Method which uses only the function evaluations to find the minimum: making it a very robust algorithm and very efficient for problems that are nonlinear or have a number of discontinuities. Our preliminary results demonstrate significant change in velocity of the blood and occurrence of vortices in the region of less elasticity and the tendency of the artery to deform minimum in the hardened less elastic

region. Our estimation results show that the parameters are identifiable. The mean square error of the estimate as a function of SNR shows accuracy of the estimation.

ACKNOWLEDGEMENT

I thank Dr. Aleksander Jeremic for giving me this opportunity to work with him and for his constant guidance and for his fruitful discussions on my research work through the course of my study.

I would like to express my sincere thanks to my *'mama'* (Mr. Subhash Dighe) and my *'mami'* (Mrs. Jayashree Dighe) for their unconditional love, support and motivation throughout my master's work.

I would like to thank my brother Vaibhav dada for making this wonderful journey a reality. My mummy and baba, sanju kaka and kaki, thank you for supporting me through all my crazy adventures in life. Trupti and Saurabh, hope you look upto and benefit from my research work. Love you all.

My grandmother *'my amma'* who laid my educational foundation, I dedicate this thesis to you.

TABLE OF CONTENTS

ABSTRACT.....iv

ACKNOWLEDGEMENT.....vii

TABLE OF CONTENTS.....viii

LIST OF FIGURES.....x

CHAPTER 1 Introduction 1

Research Outline.....5

Thesis Layout.....6

CHAPTER 2 Mathematical Modeling.....7

2.1 Modeling the Blood Flow.....7

2.1.1 Continuity Equation.....8

2.1.2 Navier Stokes Equation.....10

2.2 Boundary Conditions.....13

2.3 Modeling the Deformation in the Artery.....15

CHAPTER 3 Implementation of Mathematical Model.....22

3.1 Modeling with Comsol Multiphysics.....22

3.1.1 Homogeneous and isotropic elasticity profile.....24

3.1.2 Non Homogeneous and isotropic elasticity profile.....24

3.1.3 Non Homogeneous anisotropic elasticity profile.....25

3.2 Numerical Example for the Forward Model..... .25

CHAPTER 4 Statistical Modeling.....39

4.1 Measurement Model.....39

4.2 Statistical Model.....44

4.3 Parameter model.....47

4.3.1 Deterministic parameter model.....48

4.3.2 Deterministic Parameter Estimation.....50

4.3.3 Stochastic parameter model.....56

CHAPTER 5 Numerical Examples.....60

5.1 Performance Measure.....60

5.2 Numerical Examples.....62

5.3 Numerical Results.....64

CHAPTER 6 Conclusion and Future Work.....79

6.1 Conclusion.....79

6.2 Future Work.....80

REFERENCES.....81

LIST OF FIGURES

Fig. 2.1 Eulerian and Lagrangian Description of Motion.....9

Fig. 2.2 Deformation in the Artery.....16

Fig. 2.3 Interaction of Equations in the two models.....20

Fig. 2.4 Stress-Strain Relationship and Boundary conditions.....21

Fig. 3.1 Generalized Comsol Algorithm.....28

Fig. 3.2 Algorithm for Mathematical Model.....29

Fig. 3.3 Subdomain Geometry Plot.....30

Fig. 3.4.a Mesh Plot.....31

Fig. 3.4.b Mesh Parameters.....31

Fig. 3.5 Pulsating Pressure Plot.....32

Fig. 3.6 Artery Deformation Plot.....32

Fig. 3.7.a Blood Flow at Time T/4 sec.....33

Fig. 3.7.b Blood Flow at Time T/2 sec.....33

Fig. 3.7.c Blood Flow at Time 3T/4 sec.....34

Fig. 3.7.d Blood Flow at Time T sec.....34

Fig. 3.8 Elasticity Profile demonstrating Atherosclerosis.....35

Fig. 3.9 a Blood flow at Time T/4 sec under influence of atherosclerosis.....36

Fig. 3.9 b Blood flow at Time T/2 sec under influence of atherosclerosis.....36

Fig. 3.9 c Blood flow at Time 3T/4 sec under influence of atherosclerosis.....37

Fig. 3.9 d Blood flow at Time T sec under influence of atherosclerosis.....37

Fig. 3.10 Artery Deformation Plot under the influence of Atherosclerosis.....38

Fig. 4.1 Selection of Deforamtion Measurements.....43

Fig. 4.2 Measurement Model.....58

Fig. 4.3 Least Squares Approach.....58

Fig. 4.4 Estimation Model.....59

Fig. 5.1 MSE vs. SNR for single parameter estimation.....68

Fig. 5.2 Goodness of fit vs. SNR for one parameter estimation.....68

Fig. 5.3a $MSE(\hat{\theta}_1)$ vs. SNR for velocity measurements.....69

Fig. 5.3b $MSE(\hat{\theta}_2)$ vs. SNR for velocity measurements.....69

Fig. 5.4a $MSE(\hat{\theta}_1)$ vs. SNR for deformation measurements.....70

Fig. 5.4b $MSE(\hat{\theta}_2)$ vs. SNR for deformation measurements.....70

Fig. 5.5a $MSE(\hat{\theta}_1)$ vs. number of velocity measurements.....71

Fig. 5.5b $MSE(\hat{\theta}_2)$ vs. number of velocity measurements.....71

Fig. 5.6a $MSE(\hat{\theta}_1)$ vs. number of deformation measurements.....72

Fig. 5.6b $MSE(\hat{\theta}_2)$ vs. number of deformation measurements.....72

Fig. 5.7 Goodness of fit vs. SNR for 250 deformation points.....73

Fig. 5.8 Goodness of fit vs. SNR for 500 deformation points.....73

Fig. 5.9 Goodness of fit vs. SNR for 1000 deformation points.....74

Fig. 5.10 Goodness of fit vs. SNR for 250 velocity points.....74

Fig. 5.11 Goodness of fit vs. SNR for 500 velocity points.....75

Fig. 5.12 Goodness of fit vs. SNR for 1000 velocity points.....75

Fig. 5.13 Goodness of fit vs. SNR for 250 deformation points.....76

Fig. 5.14 Goodness of fit vs. SNR for 500 deformation points.....76

Fig. 5.15 Goodness of fit vs. SNR for 1000 deformation points.....77

Fig. 5.16 Goodness of fit vs. SNR for 250 velocity points.....77

Fig. 5.17 Goodness of fit vs. SNR for 500 velocity points.....78

Fig. 5.18 Goodness of fit vs. SNR for 1000 velocity points.....78

Chapter 1

Introduction

Blood flow in the arteries is a complex process of cellular interactions consisting of mechanical, electro-mechanical and electro-chemical components as a result analyzing the blood flow is a very difficult process. However nearly *47%* of the deaths in North America are caused by cardiovascular diseases and this has created significant research interest directed towards developing cardiovascular imaging techniques, diagnosis procedures etc. An essential and important part of these efforts is mathematical modeling that enables us to evaluate different scenarios from a clinical perspective: to obtain more accurate diagnosis of pathological conditions and from academic point of view to study the causes behind occurrence of such a condition. Modeling the blood flow is a very complicated process if done at a cellular level where we have to incorporate all the electro-mechanical and electro-chemical interactions taking place, which is not computationally feasible at this point, however to study a certain condition we need not have to necessarily focus on all the aspects of blood flow. We can focus on one particular aspect of the blood flow and try to develop an inverse model which can be useful for improved diagnosis on predicting the onset of certain pathological condition. We focus on the mechanical aspect associated with the blood flow and if we can detect the trend in the change in elasticity sufficient enough, we can take the necessary actions in prevention pathological condition such as atherosclerosis.

Blood flows through the artery under the influence of an applied pressure drop across the artery. Human blood is a suspension cells in an aqueous solution of electrolytes and non electrolytes. The blood is separated into *plasma* and *cells*. The plasma is about *90%* water, *7%* plasma protein, *1%* inorganic substances and *1%* other organic substances. The cellular contents are essentially all erythrocytes, or red cells with white cells of various categories making up less than $1/800^{th}$ of the cellular volume and platelets making up less than $1/600^{th}$ cellular volume. Normally the red cells occupy about *50%* of the blood cellular volume. The viscosity of the blood depends on the amount of suspended particles, mostly red blood cells in the blood. The viscosity of blood is generally observed [McDonalds, 1990] to range from *1.2cP* to *70cP* for different range of shear rates. In large blood vessels, whose dimensions are much larger than the dimensions of the red blood cells, the blood appears to be a homogeneous fluid and the blood in such a case is treated as a Newtonian fluid with constant coefficient of viscosity without causing a significant error on the pressure flow relationship. The blood pressure decreases as the blood moves away from the heart. The typical values of the arterial blood pressure [Fung, 1990] for a resting healthy adult human range from are approximately *120 mmHg* systolic and *80 mmHg* diastolic with significant individual variations. If the tube is elastic then high pressure end would distend more than the low pressure end. The diameter of the vessel therefore becomes non-uniform and the degree of non-uniformity depends on the flow rate. If we wish to determine the pressure flow relationship for such a system we may break the problem into two familiar components we regard the vessel to have a specified wall shape, for a given flow we compute the

pressure distribution. This pressure distribution is then applied as loading on the elastic artery, we then analyze the deformation of the artery according to the theory of elasticity for hyperelastic vessels. The result of this calculation is used to determine the boundary shape of the fluid dynamic problem. When a consistent solution is obtained the pressure distribution corresponding to a given flow and the shape of the vessel is determined. The arteries are structurally made up of connective tissue embedded in layer of smooth muscle this gives the elastic nature to the arteries. The elasticity of the arteries is observed to be in the range of 10^4-10^9 dyne/cm^2, [Mcdonalds, 1960, Bergel 1961]. In the arteries, there can be formation of abnormal regions of hardness due to a build up of fatty deposits or plaque making it to lose its elasticity. Such hardening of the arteries and the narrowing of the lumen can cause severe atheromas and even high blood pressure and blockage of the vessels. Determination of such regions can prove very beneficial if done at an earlier stage.

The forward problem associated with blood flow modeling comprises of the artery and the cardiac muscle as a hyperelastic material [Fung, 1965, Fung, 1993], and the three dimensional Navier-Stokes equations [Kundu, 2004], solves for the blood flowing through it, where we perform fluid dynamic analysis for the blood flowing through the vessel to compute the velocity at different time instances and mechanical analysis to compute the deformation of the artery which is a function of the elasticity of the vessel. The immersed boundary method [Peskin, 2002], is both a mathematical formulation and numerical scheme that employs a mixture of eulerian and lagrangian variables to model the fluid structure interaction at the boundary. It is employed to derive the equations of

motion for an elastic material. [Rosar, Peskin, 2001], used the immersed boundary method to model the flow in collapsible tubes. The equation of immersed boundary can be implemented using different numerical methods, such as the Navier-Stokes equations, that can be solved numerically for the blood flowing through the vessel using finite element method and the deformation that is computed by modeling the artery as a neo hookean case of hyperelastic material. These are well posed problems where we obtain the measurements from a model under the set of given parameters [Peskin, 2002].

Conversely, in an inverse problem we estimate the elasticity of the artery from the velocity and the deformation measurements to predict the region of atherosclerosis. In this case we have the measurements available to us and we try to predict the model parameters from these measurements. The inverse problem is actually the one that is made difficult by two characteristics. The first it does not have a unique solution i.e. the relationship between the true measurement point and the remote observations are not unique such that the same set of measurements could result from more that one parameter. The second problematic characteristic is that the problem can be ill posed. One way of improving the ill posed problem is to impose constraints on our solution which will restrict the admissible class of solutions, so that a continuous inverse exist. Some work has been done in developing inverse problems on blood flow and elasticity estimation using different modeling techniques: [Hasegawa, 2006] tried to estimate the displacement of the artery as a measure of elasticity of the artery, [Garbey, 2005], tried estimating the average blood flow and vessel location [Whiteley, 2005], localized the breast tumor by computing the coordinates of an undeformed elastic body.

Research Outline

In our study we try to develop our computational model in two main categories: First the computation of a transfer vector that establishes a relationship between the simulated and actual measurements of blood flow. Then second we develop an inverse model by solving an optimization problem by using the aforementioned transfer vector.

We outline the research approach in the following steps:

1. Develop a finite element model for the flow of blood through the artery to obtain the source to transfer measurement matrix for blood flow and deformation in the artery.
2. Perform statistical analysis on the measurement matrix obtained from our forward model.
3. Propose an inverse computational model for estimating the elasticity profile of the arterial wall.
4. Analyze the results and evaluate the performance of our estimation to infer appropriate conclusions.

Thesis Layout

This thesis comprises of six chapters. In the Chapter 2, we introduce the reader to the concepts of mathematical modeling; discuss the governing equations associated with modeling the blood flow through the arteries, the equations describing the deformation occurring in the artery and some basic assumptions associated with the modeling. Further, in Chapter 3 we implement the mathematical model described in the previous chapter, present numerical examples demonstrating the blood flowing through a branch of an artery and the behavior of blood flow in the region of atherosclerosis. Here we also provide a brief overview of the programming aspects of finite element analysis associated with the numerical computations. In the Chapter 4, we describe the statistical model, including the development of our measurement model and estimation algorithms. Then in Chapter 5, we present the applicability of our statistical model where we use numerical examples to demonstrate the performance measures of our estimators and discuss our numerical results obtained by implementation of the estimation algorithm in *MATLAB*. Our study is concluded in Chapter 6 where we also discuss the future directions for this research.

Chapter 2

Mathematical Modeling

In this Chapter, we discuss the governing equations associated with modeling the blood flow through the arteries, the equations describing the deformation occurring in the artery and some basic assumptions associated with the modeling.

2.1 Modeling the Blood Flow

As described earlier, the blood is a suspension of particles like erythrocytes that are suspended in plasma making it to behave as a non-newtonian fluid. Further, in smaller vessels of internal radius less than 0.5 mm, the changes in apparent viscosity occur, however, in the larger vessels; blood may be considered as a homogeneous fluid with a viscosity that is independent of the velocity gradient. It has been shown, [Whitemore, 1968], [Schmid-Schonbein, 1976], [Cokelet et al., 1980], [Dintenfass and Seaman, 1981] and [Dintenfass, 1985] that, in vessels in which the internal diameter is large compared with the size of the red blood cells; it behaves as a Newtonian fluid. We model one such larger section of the artery where the blood behaves as a *homogeneous*, *Newtonian* fluid. The motion of the blood in such a region of the artery is described by the continuity equation and the Navier-Stokes Equation [Kundu, 2004].

For notational simplicity, we use the Einstein's notations, where for a variable v, a *scalar* v is denoted as v, *vector* v is denoted as v_i for $i=1,2,...,n$, where v_i represents a *row vector*

and a *column vector* is represented as $(v_i)^T$. A matrix v is denoted as v_{ij} for $i=1,2,...,n$, $j=1,2,...,m$, where i is the number of rows and j is the number of columns. The matrix multiplication $a_{jk} = \sum_{j=1}^{N} u_{ij} v_{jk}$ is represented as $a_{jk} = u_{ij} v_{jk}$ and the multiplication of a matrix and a vector is represented as $a_{ij} = u_{ij} v_j$ or $a_{ij} = (v_i)^T u_{ij}$.

2.1.1 Continuity Equation

The continuity equation presents the conservation of mass law which is given by

$$\frac{1}{\rho}\frac{D\rho}{Dt} + \frac{\partial v_i}{\partial x_i} = 0 \ . \tag{2.1a}$$

The particle derivative $\frac{D\rho}{Dt}$ is the rate of change of density following the blood particle. It is made of two parts: $\partial\rho/\partial t$ which is the local rate of change of ρ at a given point and the second part is the convective derivative, $v_i \frac{\partial \rho}{\partial x_i}$ which is the change in ρ as a result of the convection of the particle from one location to another. It can be non zero because of the changes in the pressure, temperature or composition; however blood is considered to be *incompressible* in the regions where its density does not change with pressure. The continuity equation in the incompressible form reduces to

$$\frac{\partial v_i}{\partial x_i} = 0. \tag{2.1b}$$

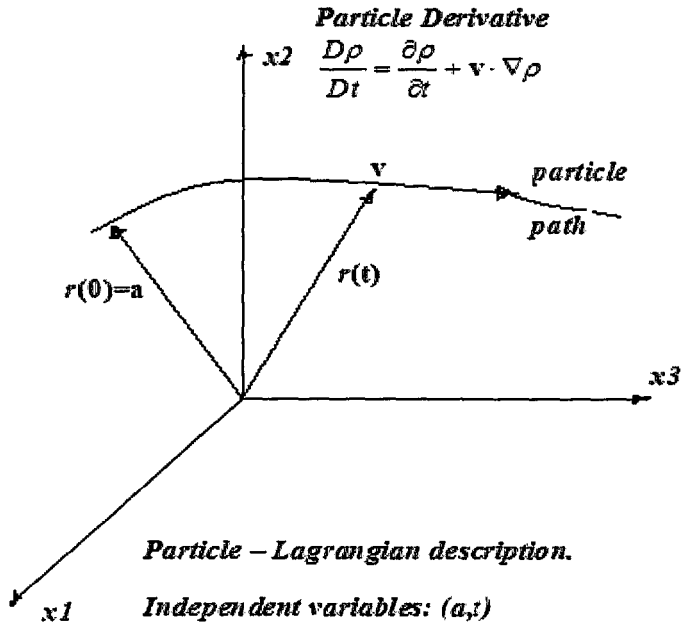

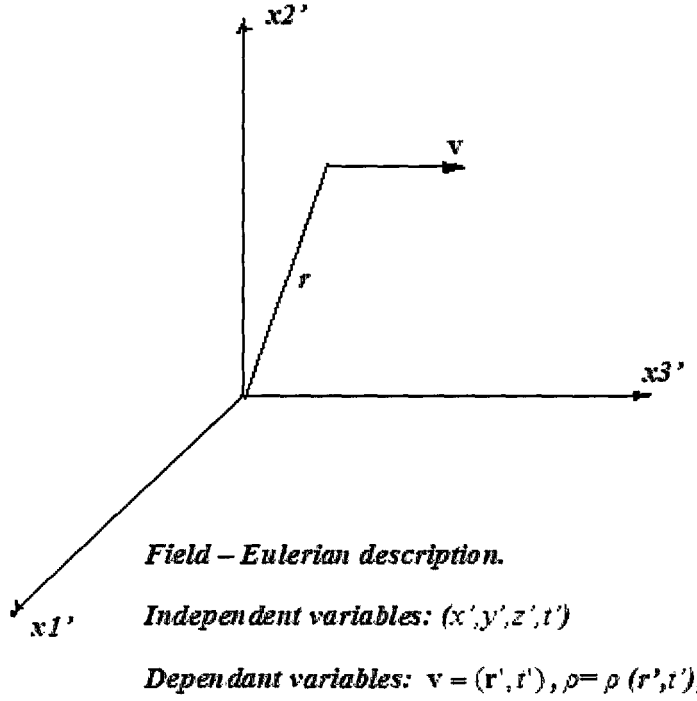

Fig. 2.1 Eulerian and Lagrangian Description of Motion, [Kundu, 2004]

2.1.2 Navier-Stokes Equation

The Navier-Stokes equation states that the changes in momentum in infinitesimal volumes of blood are simply a sum of the dissipative viscous forces, changes in pressure, gravity, and the internal forces acting inside the blood and is given by

$$\rho\frac{Dv_i}{Dt} = -\frac{\partial p}{\partial x_i} + \rho g_i + \frac{\partial}{\partial x_j}\left[2\mu \cdot e_{ij} - \frac{2}{3}\mu \cdot \left(\frac{\partial v_l}{\partial x_l}\right)\cdot \delta_{ij}\right], \tag{2.2}$$

where ρ denotes the density of blood, v denotes the velocity of blood, ρg_i is the gravitational force, the term $\frac{\partial p}{\partial x_i}$ represents the pressure gradient in a particular direction, and the Kronecker delta δ_{ij} is defined as

$$\delta_{ij} = \begin{cases} 1, \forall i = j \\ 0, \forall i \neq j \end{cases}. \tag{2.3}$$

Further, in the Navier-Stokes equation, $\frac{\partial}{\partial x_j}\left[2\mu \cdot e_{ij} - \frac{2}{3}\mu \cdot \left(\frac{\partial v_l}{\partial x_i}\right)\cdot \delta_{ij}\right]$ represents the surface forces where

$$e_{ij} \equiv \frac{1}{2}\left(\frac{\partial v_i}{\partial x_j} + \frac{\partial v_j}{\partial x_i}\right) \tag{2.4}$$

is the strain rate tensor that represents the symmetric part of the velocity gradient tensor given by

$$\frac{\partial v_i}{\partial x_j} = \frac{1}{2}\left(\frac{\partial v_i}{\partial x_j} + \frac{\partial v_j}{\partial x_i}\right) + \frac{1}{2}\left(\frac{\partial v_i}{\partial x_j} - \frac{\partial v_j}{\partial x_i}\right). \tag{2.5}$$

The anti-symmetric part here produces fluid rotation without deformation, and cannot by itself generate stress. The stresses are generated by the strain rate tensor. Here we consider a linear relationship between shear stress σ_{ij} and the strain rate e_{mn} of the type

$$\sigma_{ij} = K_{ijmn} \cdot e_{mn}, \tag{2.6}$$

where K_{ijmn} is a fourth order tensor of viscosity coefficients having 81 components, where each stress component is linearly related to all nine components of e_{ij}. We note that 81 parameters are required to describe this relationship [Aris, 1962]. However as we consider the blood to be isotropic medium and the stress tensor to be symmetric, the stress-strain relationship is independent of the rotation of the co-ordinate system, and thus K_{ijmn} has the form

$$K_{ijmn} = \lambda\delta_{ij}\delta_{mn} + \mu\delta_{im}\delta_{jn} + \gamma\delta_{in}\delta_{jm}, \tag{2.7}$$

where $\lambda, \mu,$ and γ are scalars that depend on the local thermodynamic state. As σ_{ij} is a symmetric tensor (2.6) requires that K_{ijmn} also must be symmetric in i and j. This is consistent with equation (2.7) only if $\gamma = \mu$. Thus only 2 constants λ and μ are left of the original 81 constants. Thus (2.6) becomes

$$\sigma_{ij} = 2\mu \cdot e_{ij} + \lambda \cdot e_{mm}.\delta_{ij}, \tag{2.8}$$

where $e_{mm} = \frac{\partial v_i}{\partial x_i}$ is the volumetric strain rate and the dynamic viscosity of the blood μ provides interaction between the blood and the inner wall lining of the artery.

The complete stress tensor in our case is thus described as

$$\tau_{ij} = -p\delta_{ij} + 2\mu \cdot e_{ij} + \lambda \cdot e_{mm}.\delta_{ij} \ , \tag{2.9}$$

where in addition to shear stress σ_{ij} the blood develops additional components of stress due to *thermodynamic pressure p,* these are represented as the diagonal terms of the stress tensor τ. For blood in motion this can thus be split into a part $-p\delta_{ij}$ that would exist if it were at rest and a *shear stress tensor* part σ_{ij} due to the fluid motion alone thus,

$$\tau_{ij} = -p\delta_{ij} + \sigma_{ij}. \tag{2.10}$$

2.2 Boundary Conditions

In the previous section, we have defined the continuity equation and the Navier-Stokes equation in the three directions thus we have four equations. To compute the four unknown variables: the velocity of blood in the three directions and the pressure at that point, we need to solve these four differential equations. For this we need boundary conditions. We impose the boundary conditions as the known pressure drop across the branch ends of the artery and the second being the *no-slip condition.*

The *no-slip condition* is the flow conditions at a contact surface between the artery and the blood. The blood has a tendency to adhere to the surface because of the intermolecular interactions; that is it satisfies the condition of zero relative velocity at the artery surface. There are actually two conditions: one on the normal velocity and one on the tangential velocity. When we consider an artery that confines the blood flowing through it, a kinematic condition we impose is that the particle paths cannot go into the solid. Mathematically, the requirement is that the fluid velocity perpendicular to the wall vanishes. If n_i is the local unit normal to the surface, the condition is expressed as

$$n_i v_i = 0,$$

Viscosity is responsible for the velocity component that is tangential to the wall. The *no slip condition* is velocity at the wall is given as

$$v_i = 0, \tag{2.11}$$

These conditions enter into the mathematical formulation of the flow problem thus enabling us to solve of the four unknown parameters.

2.3 Modeling the Deformation in the Artery

The deformation in the artery results as the pulsating blood flow exerts a pressure on the inner wall of the artery. We assert that the deformation can be measured only relatively with respect to some reference state in which the cross-sectional plane is considered to be undeformed. We consider the state of the beginning of the pressure pulse in the artery as the undeformed state and neglect the residual strain present in the artery. Thus every material particle P has a reference state S_0 with three coordinates a_i, $i=1,2,3$ and a neighboring particle P' has coordinates $a_i+da'_i$, when the artery is deformed the particles P,P' are moved to Q,Q' whose coordinates are x_i and $x_i+dx'_i$ respectively. The deformation in the artery is completely known if for every point we can compute

$$x_i = a_i + u_i, \qquad i = 1,2,3 \tag{2.9}$$

where u_i is the *displacement* of the particle P.

It is not practically possible to have one on one mapping of the points so we resort to computing the partial derivatives that provide the necessary information. We express this as *deformation gradient F*

$$F_{ij} = \frac{\partial u_i}{\partial x_j}. \tag{2.10}$$

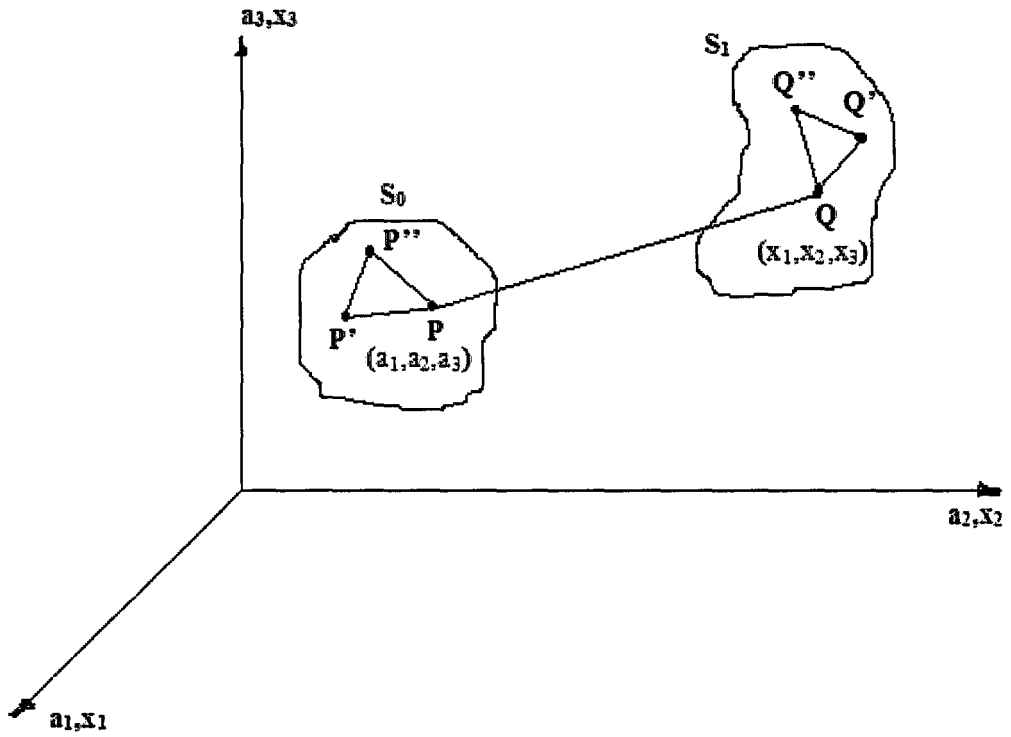

Fig. 2.2 Deformation in the Artery, [Fung, 1993]

Physically, what the deformation gradient enables us to do is to describe how the distance between two neighboring points $P(a_i),P'(a_i+da_i)$ is changed after they are deformed to $Q(x_i),Q'(x_i+dx_i)$.

The deformation gradient thus provides us with all the information about the complete deformation and the location of the artery undergoing deformation under the influence of the pressure exerted by the blood on its wall. The deformation gradient is a positive definite matrix as long as the artery is not annihilated.

To model the deformation in the artery we start with the *Green's strain tensor* E_{ij}, that characterizes the deformation near a point. [Fung, 1993; Landau, 1970]. It is given as

$$E_{ij} = \frac{1}{2}\left(\frac{\partial u_i}{\partial x_j} + \frac{\partial u_j}{\partial x_i} + \frac{\partial u_k}{\partial x_i} \cdot \frac{\partial u_k}{\partial x_j} \right). \tag{2.11}$$

The pressure exerted by the blood on the wall of the artery produces the stress in the artery that causes the artery to deform. To model the stress strain relationship, we consider the artery and cardiac muscle and to be a hyperelastic material. A hyperelastic material is characterized by its strain energy function W_{hyp}, which is the function of its strain state. The stress in such a material is computed from its strain energy function W_{hyp} as described below.

Work is done by the blood in applying the force on the wall of the artery. The force multiplied by the velocity of its travel is the power of the force. Now let us assume a blood vessel tied at one end and loaded by a force at the bottom. In the deformed state the

length of the specimen be L_0, cross-sectional area be a , the longitudinal stress is σ, so the force is $\sigma.a.$ if the length is extended by a small amount δL then the work done is $\sigma.a.\delta L.$

Hence the work done by the force per unit original volume is

$$\frac{WorkDone}{a_0 L_0} = \frac{\sigma \cdot a \cdot \delta \cdot L}{a_0 L_0}. \tag{2.12}$$

We denote the work done by the force per unit mass by the symbol δW_{hyp}, and the mass per unit volume or the initial density by ρ_0. Thus $\rho_0.\delta W_{hyp}$ is the work done or the *strain energy* per unit volume. The work energy function W_{hyp} can be expressed in of nine terms of strain components E_{ij} when the partial derivatives of W_{hyp} are formed. When such strain-energy functions exist the stress components S_{ij} can be obtained as derivatives of $\rho_0.\delta W$

$$S_{ij} = \frac{\partial(\rho_0 \cdot W)}{\partial E_{ij}}, \tag{2.13}$$

where

$$S_{ji} = J \frac{\partial a_i}{\partial x_\alpha} . \frac{\partial a_j}{\partial x_\beta} . \tau_{\beta\alpha} \tag{2.14}$$

is the Piola-Kirchoff stress. It is computed by the numerical differentiation of the strain energy function.

Thus with the expression (2.14) we establish a relationship between the Cauchy stress τ_{ij} (2.9) defined with respect to the present configuration and the Piola-Kirchoff stress defined with respect to the reference configuration of motion. For infinitesimal deformations, the Cauchy and Piola-Kirchoff stress tensors are identical.

Further, in Chapter 3 we will discuss the implementation of the forward model, the programming aspects associated with it and some related concepts of mathematical modeling.

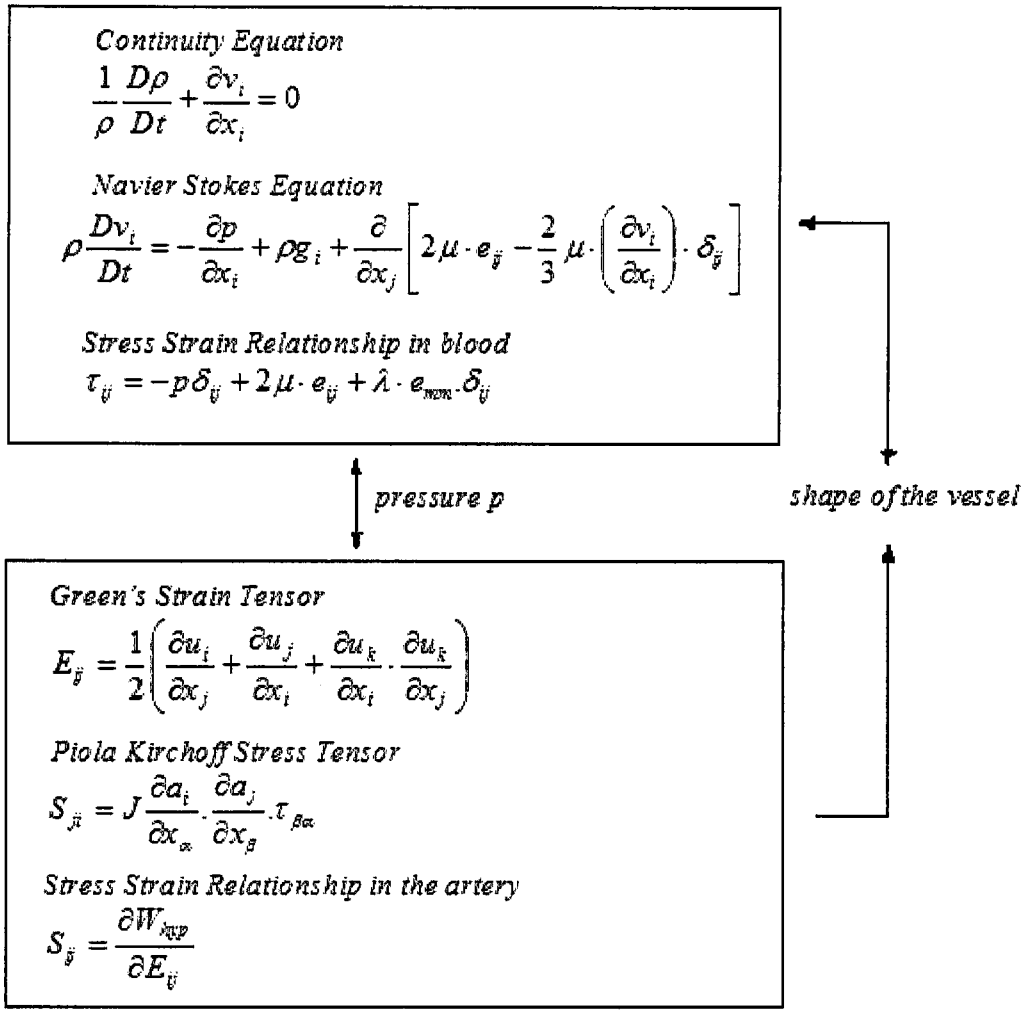

Fig. 2.3 Interaction of Equations in the two models.

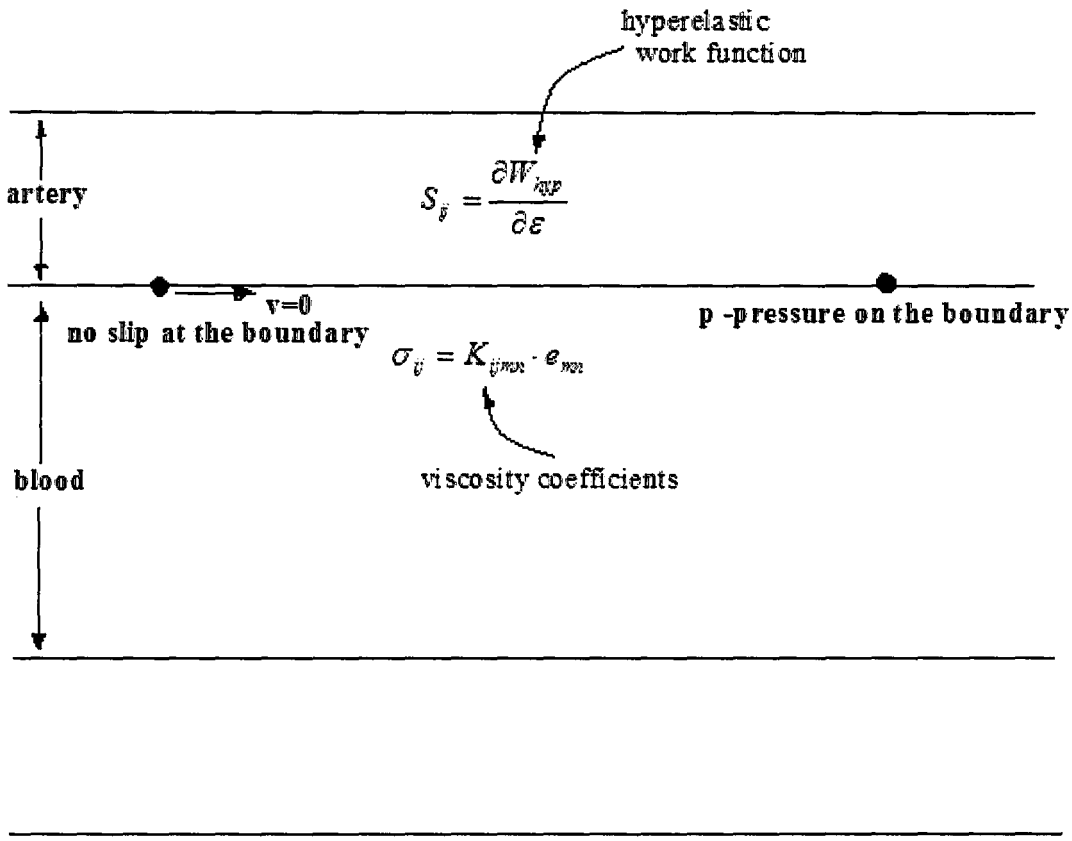

Fig. 2.4 Stress-Strain Relationship and Boundary conditions.

Chapter 3

Implementation of the Mathematical Model

In this Chapter, we implement the mathematical model described in the previous chapter, present numerical examples demonstrating the blood flowing through a branch of an artery and the behavior of blood flow in the region of atherosclerosis. Here we also provide a brief overview of the programming aspects of finite element analysis associated with the numerical computations.

3.1 Modeling with *COMSOL MULTIPHYSICS*

COMSOL MULTIPHYSICS (*FEMLAB*) is a finite element analysis and solver software package that solves different engineering problems which are formulated by partial differential equations (PDE's). The Multiphysics environment along with different modules features a variety of solvers that address complex non-linear problems formed by a combination of differential equations. *COMSOL* even provides an extensive interface to *MATLAB* which gives us the ability to export the model into the *MATLAB* environment and exploit its numerical computing techniques. It also allows for entering coupled systems of partial differential equations wherein two models can be made to interact with each other by coupling the parameters that govern the equations, for example, the pressure from the Navier-Stokes model can be used in the stress-strain model to produce the deformation in the artery as a proportion of the applied pressure.

With the *COMSOL-MATLAB INTERFACE* we intend to develop a forward model that computes numerically the flow of blood through a section of an artery under normal conditions as well as in the presence of atherosclerosis.

The Mathematical model which we refer to as the forward model consists of the pulsating blood flowing through an artery embedded in the cardiac muscle. The artery and the cardiac muscle are modeled as a hyper-elastic material modeled with the neo-hookean model, and the three dimensional Navier Stokes equation (2.2) solves for the blood flowing through it. The blood is modeled to flow under the no slip condition along the inner linings of the arterial wall. The blood flows under the influence of pulsating pressure drop [fig. 3.5] across the artery. We consider a time varying function for pressure drop, defined as

$$p(t) = \Delta p \cdot \left(\frac{3}{2} - \frac{1}{2}(\cos 2\pi t) \right), \tag{3.1}$$

where Δp is the pressure drop across the branch of the artery. Thus we perform fluid dynamic analysis for the blood flowing through the vessel to compute the velocity at different time instances. Mechanical analysis is done to compute the deformation of the artery and muscle which is a function of the elasticity of the vessel. The pressure computed from the Navier-Stokes model is provided as a boundary condition for the mechanical analysis done with the stress strain model. The two models are interconnected to each other by boundary conditions as the normal component of the surface force provides the coupling between the two models.

If we consider a section of an artery, its elasticity lies within a certain range. There are some tissues that may have a homogeneous elasticity profile over a large region of the artery, while in cases of some pathological condition like atherosclerosis the elasticity might vary drastically, and a section of non homogeneous elasticity profile is observed. To model such arteries we choose the shear modulus which is a measure of the elasticity of the artery.

3.1.1 Homogeneous and isotropic elasticity profile

The arteries have large number of sections over which the elasticity does not change significantly. Such regions can be modeled have an elasticity profile that does not change from one point to another and is the same at a given point in all directions. Such an elasticity profile can be modeled as

$$G(r) = g, \tag{3.2}$$

where g is the constant shear modulus.

3.1.2 Non Homogeneous and isotropic elasticity profile

There are regions in the artery where the elasticity changes considerably along its length. To model such regions we can have an elasticity profile that changes spatially and can be expressed as function of a linear combination of different spatial basis functions

$$G_i(r) = \sum_{i=1}^{q} g_i \cdot f_i(r), \tag{3.3}$$

where q is the number of unknown basis functions and $f_i(r)$ are the spatial basis functions modeling spatial variations.

3.1.3 Non Homogeneous anisotropic elasticity profile

The arteries are complex cardiovascular tissues whose structure can vary quite significantly from region to region. To model such complexity in structure we need a more detailed representation of the elasticity profile, which changes from one point to another and is different in different directions as well. For example, we can model the shear modulus that has different shear components in different directions. This can be done by explicitly specifying 36 components of the compliance matrix that expresses the relationship between the stress and the strain.

3.2 Numerical Example for the Forward Model

We create a numerical example to implement the forward mathematical model. In this numerical example we take into consideration the condition when the blood flows through the artery without any irregularities in the hardening of the vessel and the case when there is atherosclerosis present in the artery. Note that we are simulating the measurements for the blood flow to validate that the elasticity parameters can be estimated and that the inverse model implemented later is applicable and can be used in realistic clinical environment.

For implementing the mathematical model we set the density of blood ρ = *1060 kg/m,* viscosity of blood η = *0.005 Pa-s,* and vary the pulsating pressure from *8000 to 16000 Pa.* [Fung, 1990] modeled as a time varying cosine function of the pressure drop across the artery. The cardiac muscle and the artery have the poisson's ratio $\nu = 0.5$, [Fung, 1990]. Furthermore, we consider the artery and the cardiac muscle to be a case of homogeneous, isotropic hyperelastic material. By this we mean that the third invariant of the right Cauchy Green tensor, $C=FF^T$ (2.10) is equal to 1, and the poisson's ratio $\nu = 0.5$, [Fung, 1990]. The stored energy function $W_{hyp} = W_{hyp}(I_1, I_2)$, can be expressed in the polynomial form [Fung, 1993; Fung, 1990] as

$$W_{hyp} = \sum_{i=0,j=0}^{\infty} C_{ij}(I_1 - 3)^i (I_2 - 3)^j, \tag{3.4}$$

where I_1 and I_2 are the invariants of the right Cauchy Green tensor. For different values of i and j different hyperelastic models are obtained. We use the simplest and the most widely used *neo-hookean model* [Fung, 1993; Fung, 1990].

$$W_{hyp} = C_{10}(I_1 - 3). \tag{3.5}$$

where I_1 is the trace of right Cauchy Green tensor C, and the constant $C_{10} = \frac{1}{2}.G$ where G is the shear modulus. The cardiac muscle is modeled to have a constant shear modulus G = *7e5 Pa*. The artery is modeled to have a homogeneous and isotropic elasticity profile as described in (3.2) with shear modulus *6e6 Pa,* and the atherosclerosis region is

modeled with non homogeneous and isotropic elasticity profile (3.3). In this case, we choose spatially varying exponential basis function having a decay constant $\alpha = 2$, and the shear modulus varying in the range between *6e6 Pa* to *8e6 Pa.* [Fung, 1993].

The blood-vessel geometry structure available to us as a parasolid file, is imported into the *COMSOL* environment. The structure being divided into three subdomains [fig 3.3] models the blood, artery and the cardiac muscle. Meshing the geometry with tetrahedral elements enables us to create a finite element model with degrees of freedom as illustrated in [fig 3.4] along with the size and the number of elements. We create a relatively finer mesh in the region of interest to study the deformation and the flow with better accuracy where as resort to a relatively coarser mesh in the outer less important region of cardiac muscle to save the time on computation.

To solve the model we use the time dependant *'SPOOLES'* solver provided in the *COMSOL* package which works on the general systems of the form Ax = b using the multi-frontal method and the direct LU factorization of the sparse matrix A. [Ashcraft, 1999].

The rigidity profile [fig 3.8] shows the elastic behavior of the artery and the deformation plots [fig 3.6 and fig 3.10] enables us to study the deformation as a result of abnormal hardening in the artery. The irregularities in the blood flow in presence of atherosclerosis [fig 3.9] can be compared with the normal flow of blood [fig 3.7].

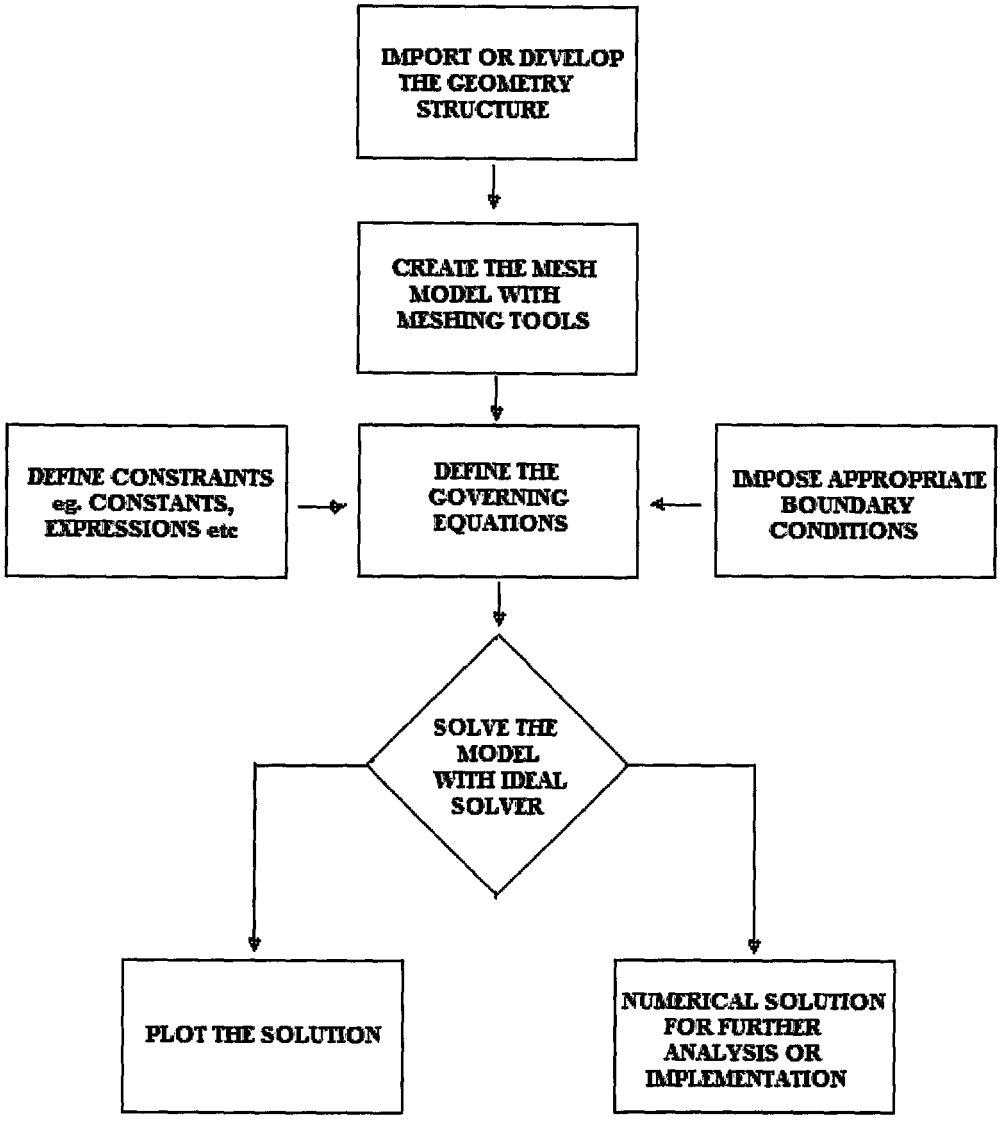

Fig. 3.1 Generalized Comsol Algorithm.

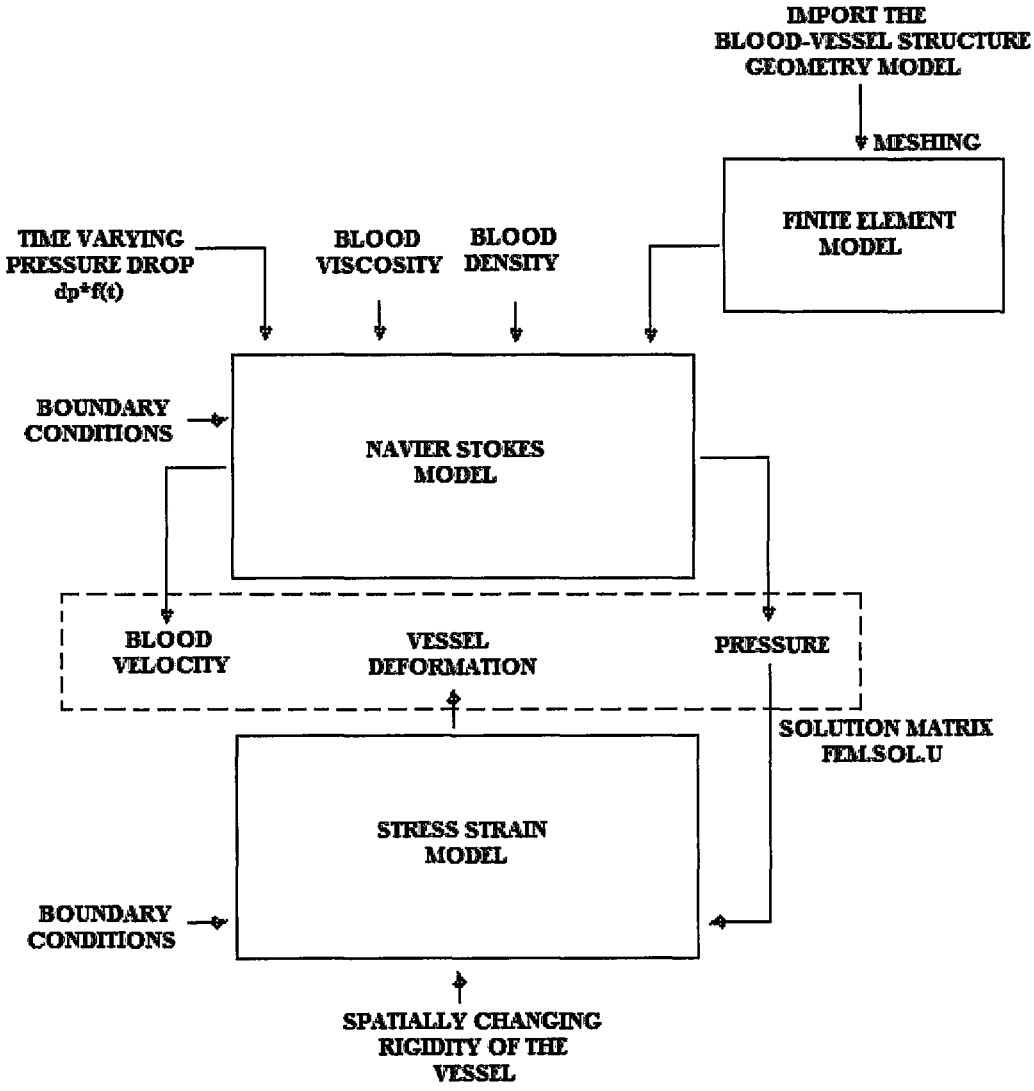

Fig. 3.2 Mathematical Model.

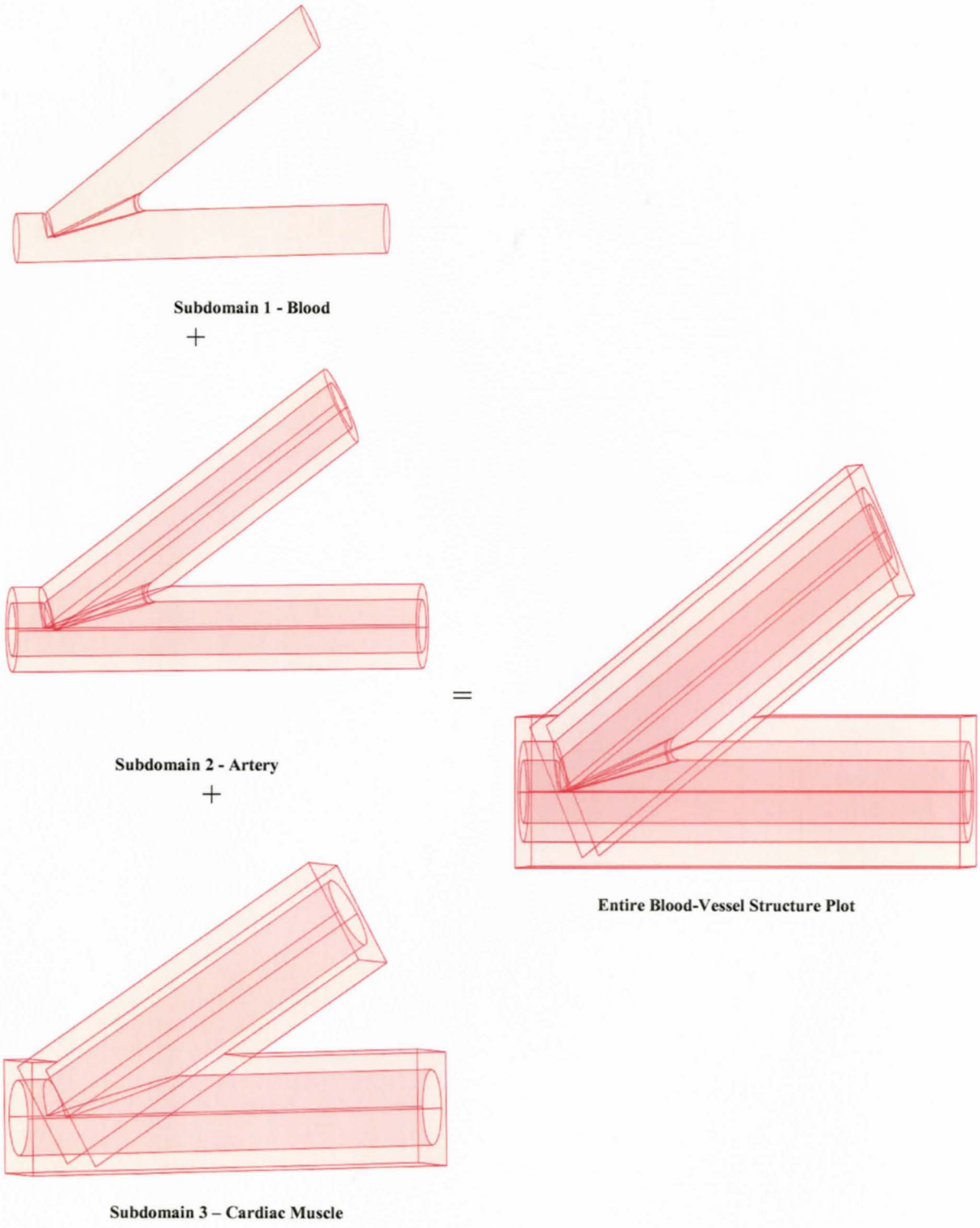

Fig. 3.3 Subdomain Geometry Plot.

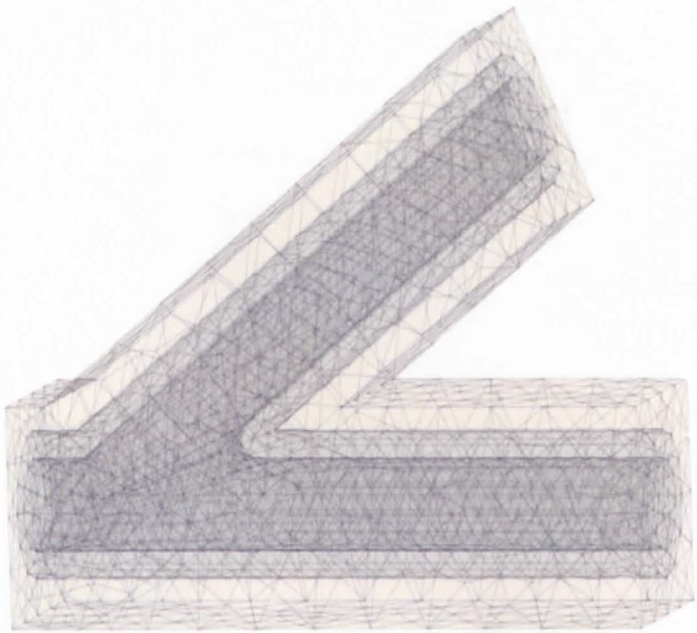

Fig. 3.4.a Mesh Plot.

Number of degrees of freedom	**22663**
Number of mesh points	**857**
Number of tetrahedral elements	**4162**
Number of boundary elements	**1670**
Number of edge elements	**346**
Number of vertex elements	**52**
Minimum element quality	**0.1881**

Fig. 3.4.b Mesh Parameters.

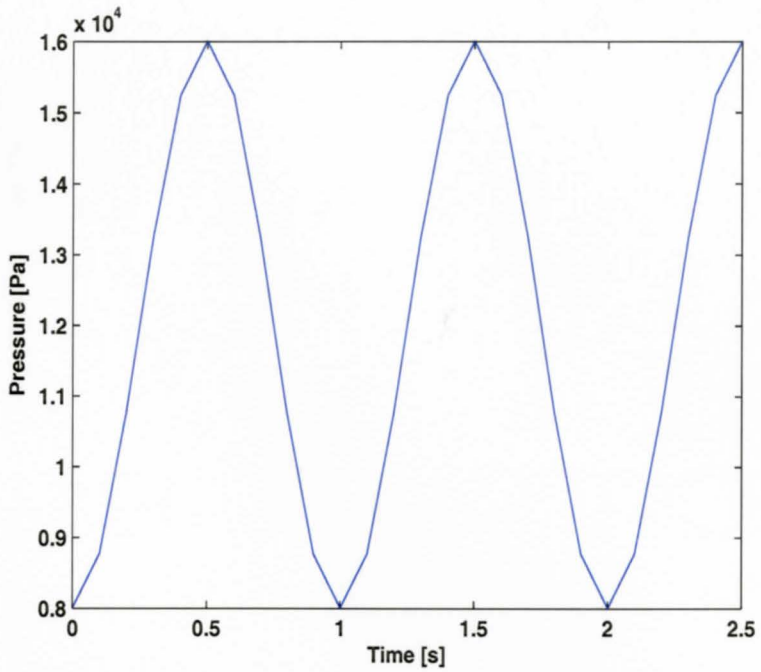

Fig. 3.5 Pulsating Pressure Plot.

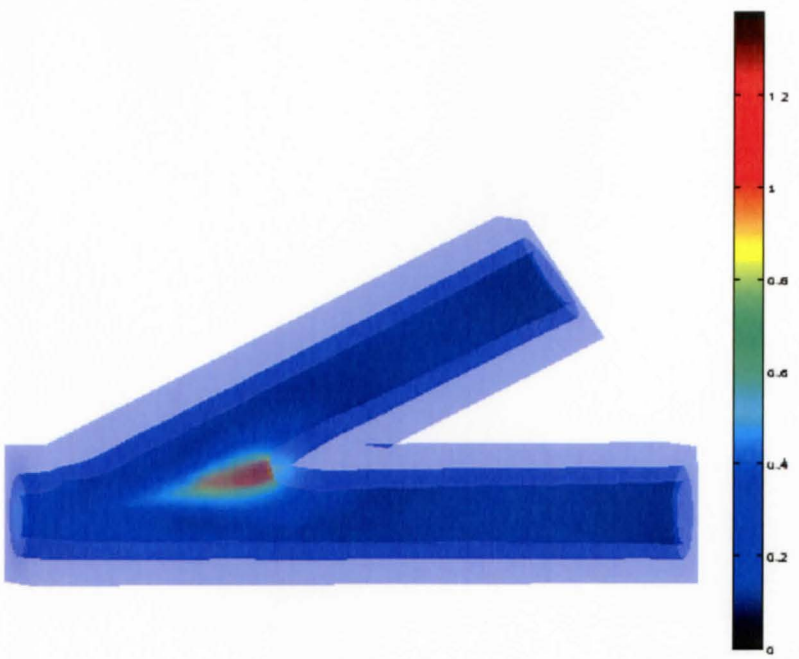

Fig. 3.6 Artery Deformation Plot.

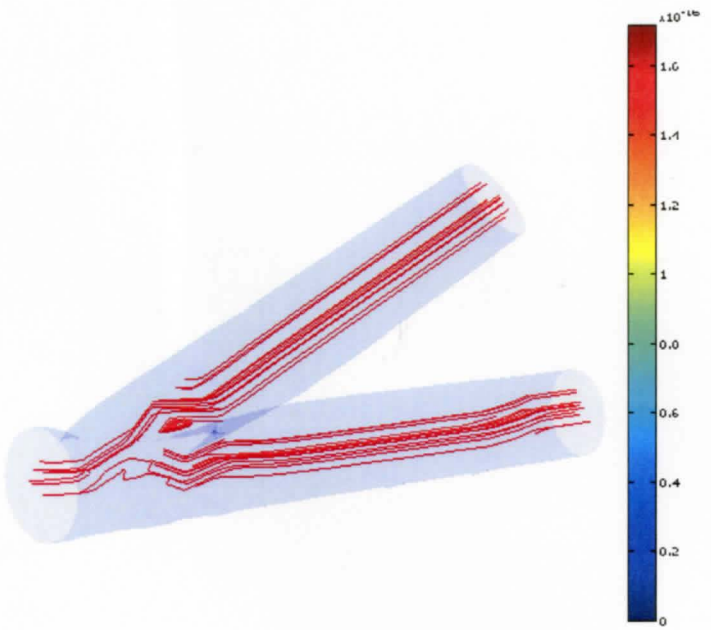

Fig. 3.7.a Blood Flow at Time T/4 sec.

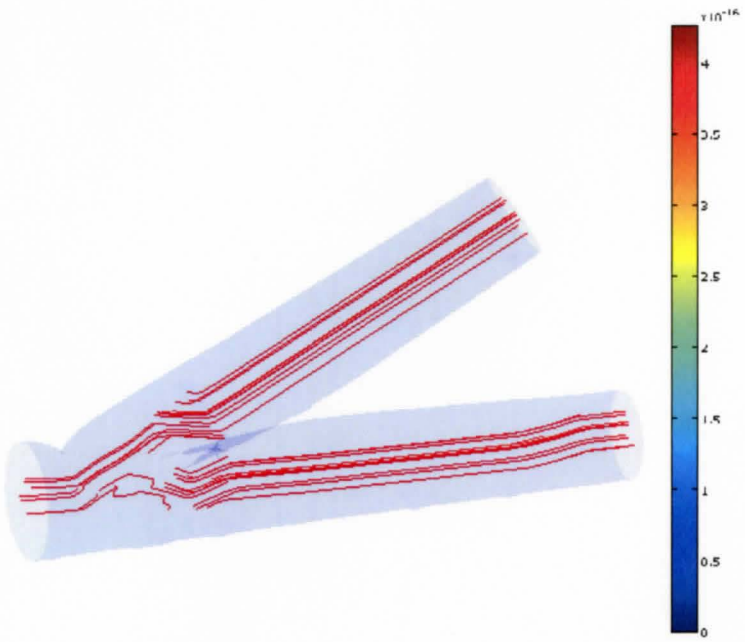

Fig. 3.7.b Blood Flow at Time T/2 sec.

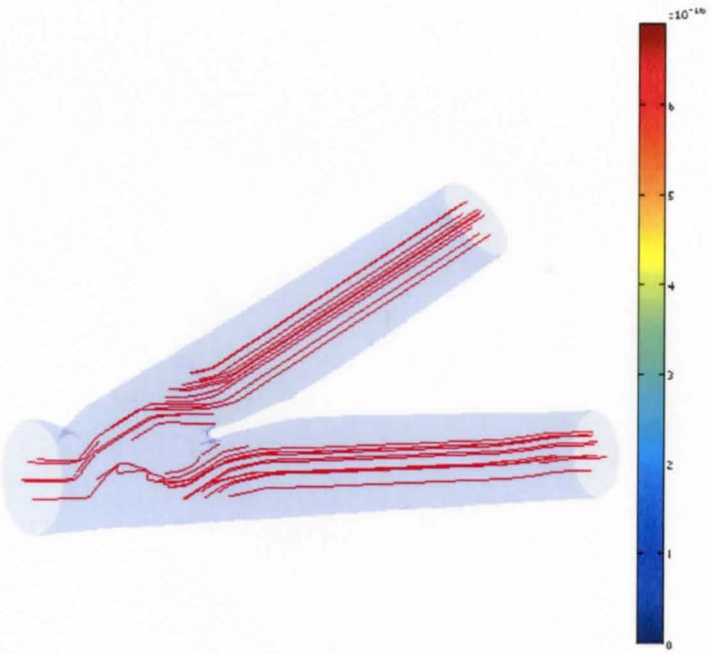

Fig. 3.7.c Blood Flow at Time 3T/4 sec.

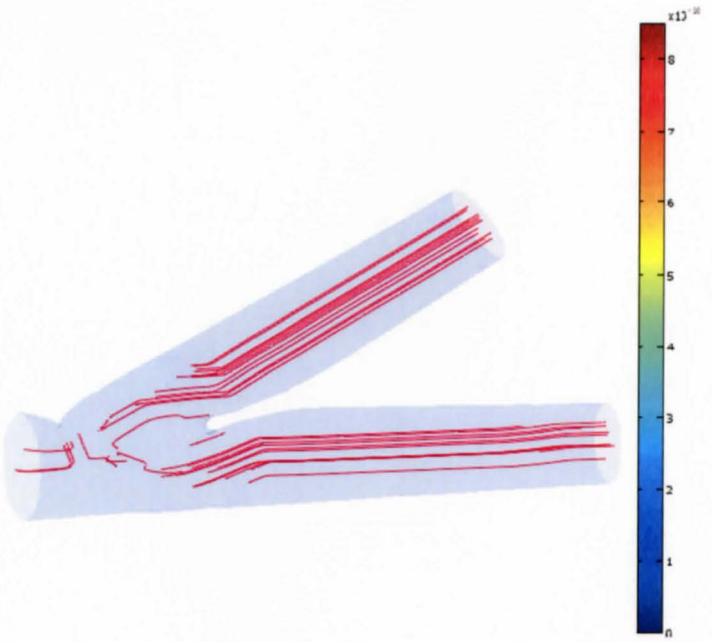

Fig. 3.7.d Blood Flow at Time T sec.

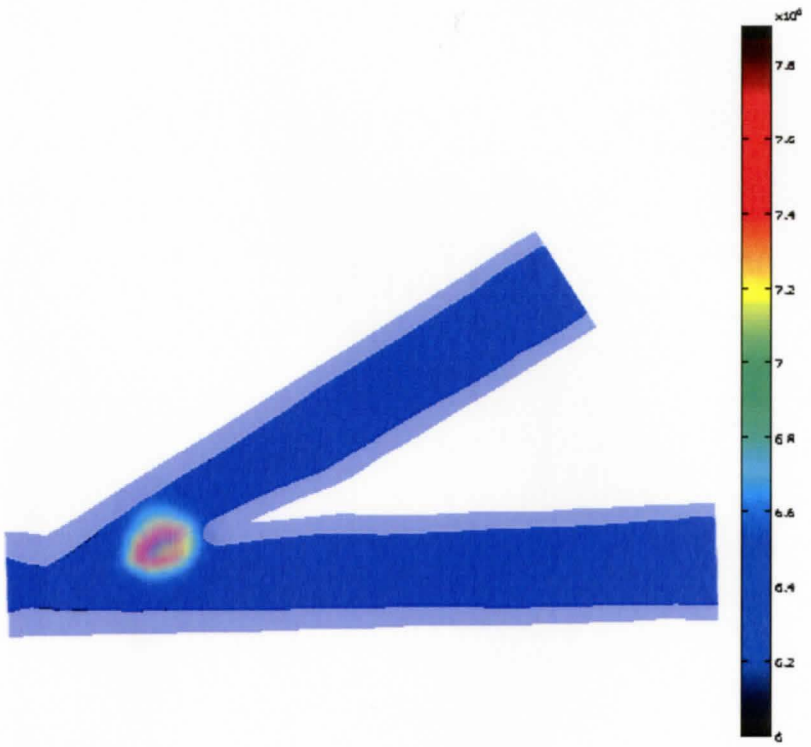

Fig. 3.8 Elasticity Profile demonstrating Atherosclerosis.

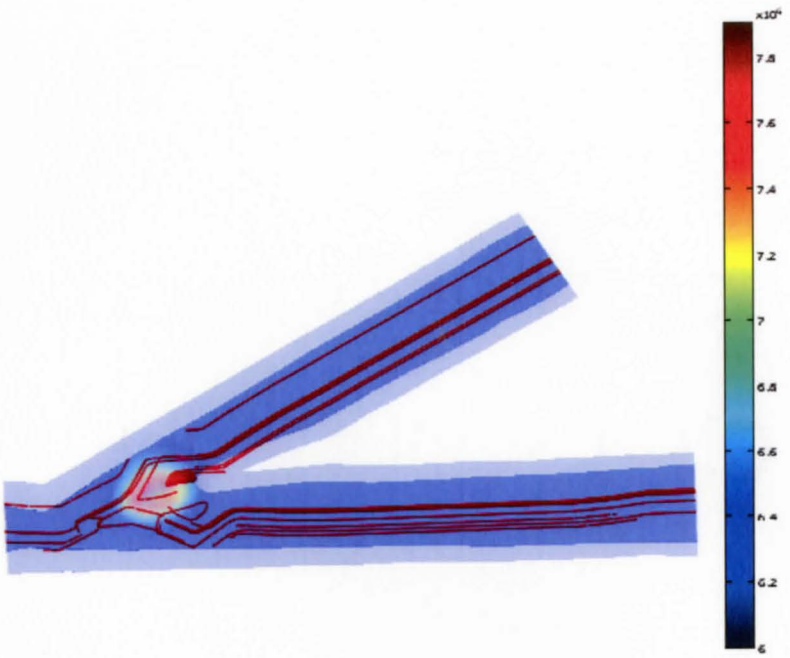

Fig. 3.9 a Blood flow at Time T/4 sec under influence of atherosclerosis.

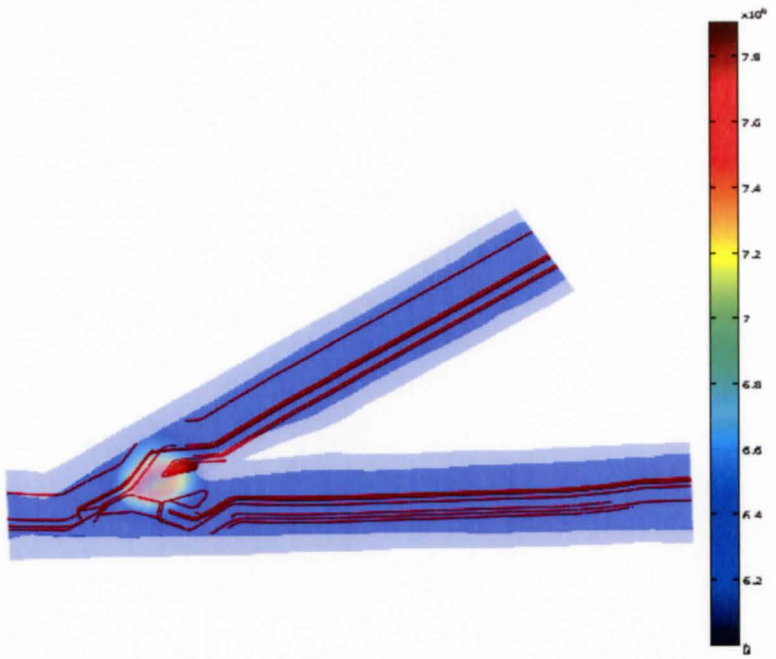

Fig. 3.9 b Blood flow at Time T/2 sec under influence of atherosclerosis.

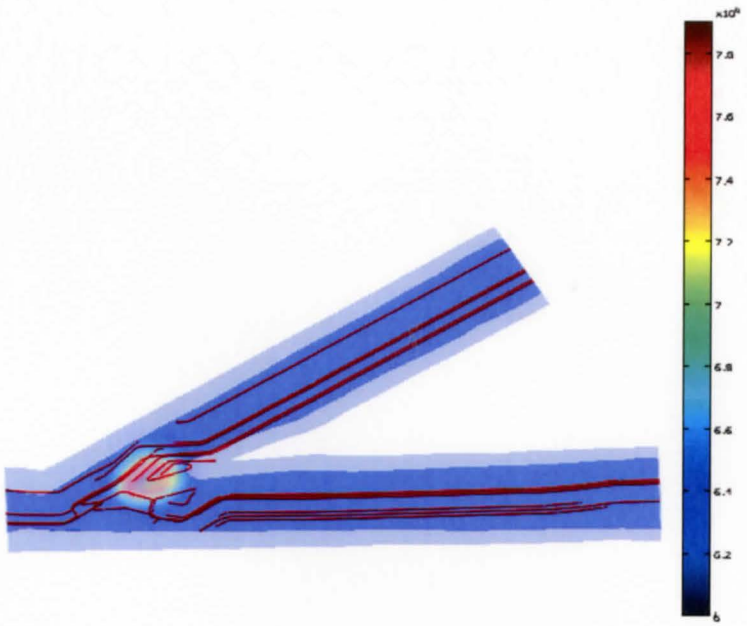

Fig. 3.9 c Blood flow at Time 3T/4 sec under influence of atherosclerosis.

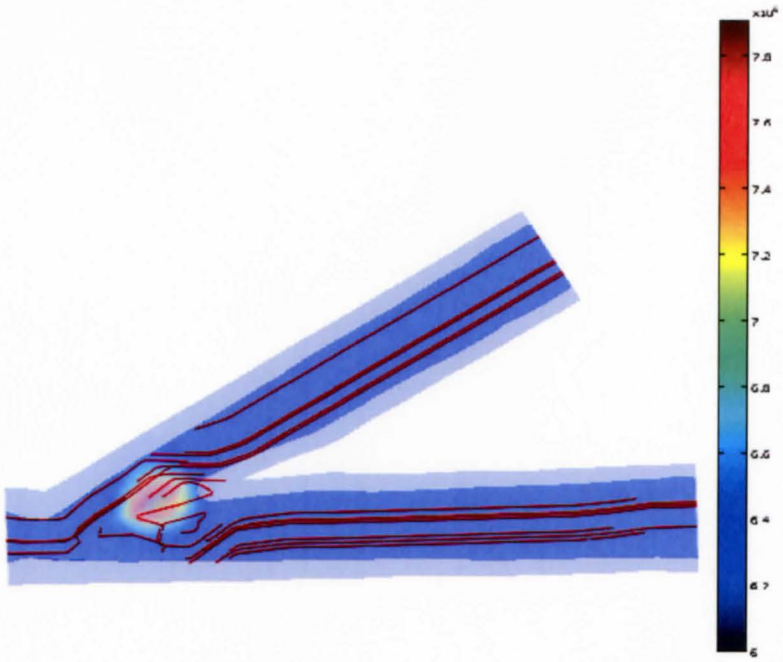

Fig. 3.9 d Blood flow at Time T sec under influence of atherosclerosis.

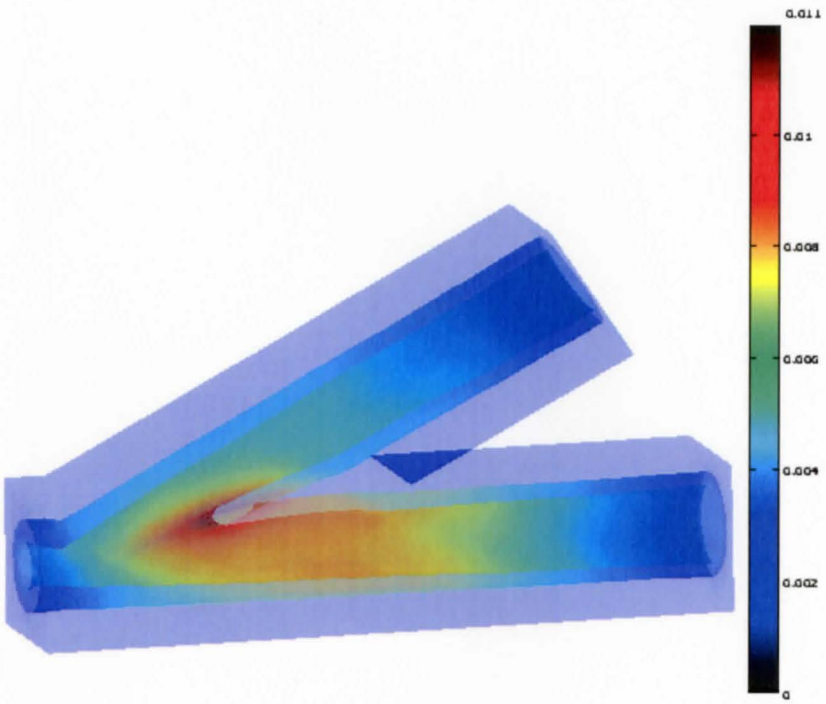

Fig. 3.10 Artery Deformation Plot under the influence of Atherosclerosis.

Chapter 4

Statistical Modeling

In this Chapter, we propose a statistical model for the simulated measurements obtained from the *Forward Mathematical Model* described in the earlier chapters, and use the inverse modeling technique to predict the atherosclerosis affected region in the artery.

4.1 Measurement Model

We obtain measurements from the finite element model that is used to simulate the experiments or the imaging process. Finite element model with large number of point and some what realistic elasticity parameters can be used to simulate the actual experimental measurements. In realistic measurements we always have an inherent occurrence of measurement noise. This noise may be due to our inability to obtain the measurements accurately such as an uncertainty in the data acquisition process or may be a result of experimental limitation such as in tagged MRI we only have a certain degree of knowledge about where the displacement can be obtained or in case of Doppler ultrasound the images are obtained with a certain resolution. Thus when we obtain the measurements for velocity by Doppler ultrasound method we have noise and sources of errors in measurement of velocity by the Doppler ultrasound method [Gill, 1985]. In addition there are technological constraints that we need to consider when we simulate the data measurements such as, the spatial resolution of the Doppler ultrasound

[Cristopher, Starkoski, 1996]. We take into consideration the spatial resolution by confining ourselves to selecting the velocity measurements at n_v number of points. To model the noise in our measurement we use the *multivariate analysis of variance (MANOVA)* [Vonesh and Chinchilli, 1997], where for velocity measurements at r_i location for instance t_j of the period length T is given as

$$\mathbf{y}_v(\mathbf{r}_i,\mathbf{t}_j)=\mathbf{a}_v(\mathbf{r}_i,\mathbf{t}_j)+\boldsymbol{\varepsilon}_v(\mathbf{r}_i,\mathbf{t}_j),\ i=1,2,3,\ j=1,2,...p, \tag{4.1}$$

where $\mathbf{y}_v$ is the velocity measurement vector, $\boldsymbol{a}_v$ is the source to transfer measurement matrix obtained from the *COMSOL* forward model discussed in the previous chapters that we export into the *MATLAB* environment and perform statistical analysis by introducing noise $\boldsymbol{\varepsilon}_v$.

Thus the lumped velocity measurement vector for n_v number of velocity measurement points can be written as

$$\mathbf{y}_v(\mathbf{t}_j)=\left(\mathbf{y}_v(\mathbf{r}_1,\mathbf{t}_j)^T,\mathbf{y}_v(\mathbf{r}_2,\mathbf{t}_j)^T,..,\mathbf{y}_v(\mathbf{r}_{n_v},\mathbf{t}_j)^T\right)^T, \tag{4.2}$$

$$\mathbf{a}_v(\mathbf{t}_j)=\left(\mathbf{a}_v(\mathbf{r}_1,\mathbf{t}_j)^T,\mathbf{a}_v(\mathbf{r}_2,\mathbf{t}_j)^T,..,\mathbf{a}_v(\mathbf{r}_{n_v},\mathbf{t}_j)^T\right)^T,$$

$$\boldsymbol{\varepsilon}_v(\mathbf{t}_j)=\left(\boldsymbol{\varepsilon}_v(\mathbf{r}_1,\mathbf{t}_j)^T,\boldsymbol{\varepsilon}_v(\mathbf{r}_2,\mathbf{t}_j)^T,..,\boldsymbol{\varepsilon}_v(\mathbf{r}_{n_v},\mathbf{t}_j)^T\right)^T,$$

$$\therefore \mathbf{y}_v(\mathbf{t}_j)=\mathbf{a}_v(\mathbf{t}_j)+\boldsymbol{\varepsilon}_v(\mathbf{t}_j)\ ,\ j=1,2,...,p\ . \tag{4.3}$$

Further the deformation measurements are assumed to be obtained from MRI tagging method [Reichek 1999] where speckles in the tissue are used as reference markers and the deformation is calculated as a measure of the displacement of these speckles from their original location. These measurements are not available with such precise accuracy as the velocity measurements obtained from the Doppler ultrasound method. To take this into consideration in our simulated measurements, we restrict ourselves to considering the deformation measurements for considerably less number of points than the velocity measurements. We do this by dividing the geometry into s number of sections as illustrated in [fig 4.1]. Thus for every n measurement points of a particular section we select a certain percent of those n points of measurements for our estimation model. This way we can be flexible in dividing the geometry in a number of sections as well as the percentage of measurements we want to choose from a particular section. Thus we have the deformation measurements at r_i location for instance t_j of the period length T given as

$$\mathbf{y}_u(\mathbf{r}_i,\mathbf{t}_j)=\mathbf{a}_u(\mathbf{r}_i,\mathbf{t}_j)+\boldsymbol{\varepsilon}_u(\mathbf{r}_i,\mathbf{t}_j),\ i=1,2,3,\ j=1,2,...p, \tag{4.4}$$

where $\mathbf{y}_u$ is the deformation measurement vector, $\boldsymbol{a}_u$ is the source to transfer measurement matrix and $\boldsymbol{\varepsilon}_u$ is the noise in the measurement of deformation.

Thus the lumped deformation measurement vector for n_u number of deformation measurement points can be written as

$$\mathbf{y}_u(\mathbf{t}_j)=\left(\mathbf{y}_u(\mathbf{r}_1,\mathbf{t}_j)^T,\mathbf{y}_u(\mathbf{r}_2,\mathbf{t}_j)^T,...,\mathbf{y}_u(\mathbf{r}_{n_u},\mathbf{t}_j)^T\right)^T, \tag{4.5}$$

$$\mathbf{a}_u(\mathbf{t}_j) = \left(\mathbf{a}_u(\mathbf{r}_1, \mathbf{t}_j)^T, \mathbf{a}_u(\mathbf{r}_2, \mathbf{t}_j)^T, .., \mathbf{a}_u(\mathbf{r}_{n_u}, \mathbf{t}_j)^T\right)^T,$$

$$\boldsymbol{\varepsilon}_u(\mathbf{t}_j) = \left(\boldsymbol{\varepsilon}_u(\mathbf{r}_1, \mathbf{t}_j)^T, \boldsymbol{\varepsilon}_u(\mathbf{r}_2, \mathbf{t}_j)^T, .., \boldsymbol{\varepsilon}_u(\mathbf{r}_{n_u}, \mathbf{t}_j)^T\right)^T,$$

$$\therefore \mathbf{y}_u(\mathbf{t}_j) = \mathbf{a}_u(\mathbf{t}_j) + \boldsymbol{\varepsilon}_u(\mathbf{t}_j), \; j=1,2,...,p. \tag{4.6}$$

Thus we have the deformation and the velocity measurements, however we want to use these measurements so that we can fit the measurement data with the model data and develop a technique to minimize the error between the two measurements. For this we need to process the data together, so we combine the measurements together as they both play an important role our parameter estimation. The entire measurement matrix is thus a combination of n_v velocity measurements, n_u deformation measurements for different time instances with noise incorporated in them. Thus we have

$$\mathbf{y}(\mathbf{t}_j) = \left(\mathbf{y}_u(\mathbf{t}_j)^T, \mathbf{y}_v(\mathbf{t}_j)^T\right)^T, \tag{4.7}$$

$$\mathbf{a}(\mathbf{t}_j) = \left(\mathbf{a}_u(\mathbf{t}_j)^T, \mathbf{a}_v(\mathbf{t}_j)^T\right)^T,$$

$$\boldsymbol{\varepsilon}(\mathbf{t}_j) = \left(\boldsymbol{\varepsilon}_u(\mathbf{t}_j)^T, \boldsymbol{\varepsilon}_v(\mathbf{t}_j)^T\right)^T,$$

$$\therefore \mathbf{y}(\mathbf{t}_j) = \mathbf{a}(\mathbf{t}_j) + \boldsymbol{\varepsilon}(\mathbf{t}_j), \; j=1,...,p. \tag{4.8}$$

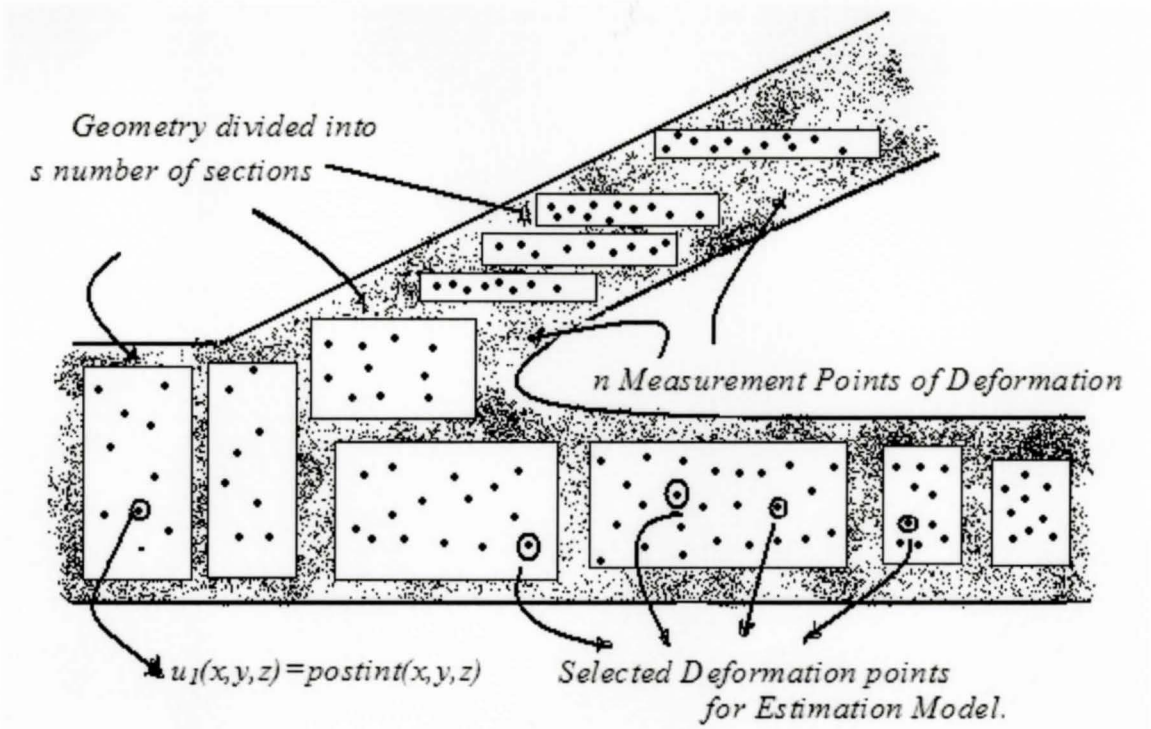

Fig. 4.1 Selection of Deforamtion Measurements.

4.2 Statistical Model

In the previous section, we incorporated the noise in our measurements now we want to study the characteristics of the noise and how the noise affects the measurements. Hence here we discuss the noise model associated with the measurements in velocity and deformation. For both our deformation and velocity measurements, we assume the noise to be Gaussian with mean zero and variance σ_u^2 and σ_v^2 respectively. We consider that there is no correlation of noise in the measurements from one measurement point to another, i.e. the measurements are spatially uncorrelated and there is no correlation of noise at one time instance with another, i.e. the measurements are temporally uncorrelated. For such a case the covariance is expressed as

$$E\left(\boldsymbol{\varepsilon}_u\left(\mathbf{r}_i,\mathbf{t}_j\right)\cdot\boldsymbol{\varepsilon}_u\left(\mathbf{r}_{i'},\mathbf{t}_{j'}\right)^T\right)=\Sigma_u\cdot\delta\left(i-i'\right)\cdot\delta\left(j-j'\right), \tag{4.9}$$

where $\boldsymbol{\varepsilon}_u$ represents the noise present in the deformation measurement at r_i and $r_{i'}$ for time instances t_j and $t_{j'}$. Further, we consider that there is no correlation in the deformation measurements in different directions the covariance matrix in this case becomes a diagonal matrix of the variance σ_u^2, thus

$$\Sigma_u=\sigma_u^2\cdot I_3, \tag{4.10}$$

and the delta function is denoted as

$$\delta(i-i') = \begin{cases} 1, i = i' \\ 0, i \neq i' \end{cases}, \tag{4.11}$$

and

$$\delta(j-j') = \begin{cases} 1, j = j' \\ 0, j \neq j' \end{cases}. \tag{4.12}$$

Similarly, for the velocity measurements, we consider that there is no correlation of noise in the measurements from one measurement point to another, i.e. the measurements are spatially uncorrelated and there is no correlation of noise at one time instance with another time instance, i.e. the measurements are temporally uncorrelated. For such a case the covariance is expressed as

$$E\left(\boldsymbol{\varepsilon}_v(\mathbf{r}_i, \mathbf{t}_j) \cdot \boldsymbol{\varepsilon}_v(\mathbf{r}_{i'}, \mathbf{t}_{j'})^T\right) = \Sigma_v \cdot \delta(i-i') \cdot \delta(j-j'), \tag{4.13}$$

where $\boldsymbol{\varepsilon}_v$ represents the noise present in the velocity measurement at r_i and $r_{i'}$ for time instances t_j and $t_{j'}$. We consider that there is no correlation in the measurements in different directions thus the covariance matrix is a diagonal matrix of the variance σ_v^2, thus

$$\Sigma_v = \sigma_v^{\,2} \cdot I_3. \tag{4.14}$$

As the two measurements are obtained independently from two different methods, we consider that there is no correlation in the measurements of the velocity and deformation thus we have,

$$E\left(\boldsymbol{\varepsilon}_u\left(\mathbf{r}_i,\mathbf{t}_j\right)\cdot\boldsymbol{\varepsilon}_v\left(\mathbf{r}_{i'},\mathbf{t}_{j'}\right)^T\right)=0. \tag{4.15}$$

To obtain the statistical distribution of our lumped model we observe that

$$E\left(\boldsymbol{\varepsilon}\left(\mathbf{t}_j\right)\cdot\boldsymbol{\varepsilon}\left(\mathbf{t}_{j'}\right)^T\right)=\Sigma\cdot\delta\left(j-j'\right), \tag{4.16}$$

where $\Sigma=\begin{bmatrix}\Sigma_u\otimes I_{n_u} & 0\\ 0 & \Sigma_v\otimes I_{n_v}\end{bmatrix}$, or using assumption of directional independence the Σ reduces to

$$\Sigma=\begin{bmatrix}\sigma_u^2\cdot I_{n_u} & 0\\ 0 & \sigma_v^2\cdot I_{n_v}\end{bmatrix}. \tag{4.17}$$

The distribution of our measurement is therefore,

$$\mathbf{y}\left(\mathbf{t}_j\right)\sim N\left(\mathbf{a}\left(\mathbf{t}_j\right),\Sigma\right). \tag{4.18}$$

4.3 Parameter model

When we perform an experiment on an individual like estimating the region of hardening in the artery it is most likely that we do not have any knowledge about the person's physical condition, in such a case the parameter is considered to be deterministic. This is the *Classical estimation* where consider to have no prior knowledge about the estimate. Further, we can have a range of elasticity of the artery to come from a particular distribution of measurements that can be obtained from experimental study, thus we consider to have apriori knowledge on the values of the parameter that helps us to predict the outcome with better accuracy in estimation. If it comes from a population then one person from that population is treated as a stochastic case. This is the *Bayesian estimation* approach that uses the distribution of unknown parameters to minimize the error between the parameter estimates. However we are interested in designing a model that takes the measurements of a person and predicts the outcome of the experiment for that particular individual. Ideally, when we consider a parameter model in the inverse study we would treat everything as deterministic unknown unless we have a strong reason to believe that the parameter comes form a particular distribution or increases our estimation efficiency by reducing our computation time. Thus we can view the unknown parameter as either *deterministic* (completely unknown) or a *stochastic* (known with a certain apriori knowledge).

4.3.1 Deterministic parameter model

In a general scenario, we would like to consider the ideal case where we have no knowledge about the parameters, where we measurements that are collectively expressed as the measurement vector as discussed in section 4.1.

In order to estimate the unknown physical parameters we first propose a parametric model corresponding to our measurement and statistical models. We will consider two cases: a. homogeneous model i.e. where the parameters do not change in space, and b. non homogeneous model i.e. the parameters are spatially dependant.

There are certain tissues that may have a homogeneous elasticity profile over a large region of the artery or the change in its elasticity varies very slightly across the cross section such that it is cannot be feasible to estimate that change. In such a case, we consider our parameter to be modeled to have a uniform elasticity profile over the range of the artery

$$G(r) = g, \tag{4.19}$$

where g is the constant shear modulus. Note that for in a homogeneous case our parameter is a constant i.e. scalar.

$$\boldsymbol{\theta} = [g]. \tag{4.20}$$

However there are certain pathological conditions such as atherosclerosis where the elasticity changes drastically in a small region of the artery. To model such nature of the artery we need to consider a non homogeneous profile for the elasticity. We model the non homogeneity by spatially varying the shear modulus, where we use a linear combination of a set of known basis functions with unknown corresponding coefficients to demonstrate the spatial linear nature of the parameter.

$$G_i(r) = \sum_{i=1}^{q} g_i \cdot f_i(r), \tag{4.21}$$

where q is the number of unknown coefficients and $f_i(r)$ are the unknown basis functions modeling spatial variations. Thus by using a linear combination of a number of functions we model the variations in elasticity as in general change in elasticity over a small region can be modeled by infinitely many such functions. Further, we can have a parameter model may potentially provide us with better estimates if we model the basis function itself, that can better fit the data. For example we have a set of exponential functions that model the basis function, where, by choosing a number of different decay constants in the basis function we can obtain better estimates. Thus we can have an elasticity profile changing spatially where a set of basis functions are known upto a parameter vector with unknown corresponding coefficients.

$$G_i(r) = \sum_{i=1}^{q} g_i \cdot f_i(r, \alpha_i). \tag{4.22}$$

Thus unknown number of parameters in the model is dependant on the number of basis functions and the parameter vector θ can be expressed as a function of the unknown parameters given by

$$\theta = \left[g_1, g_{2,\ldots,} g_q, \alpha_1, \alpha_{2,\ldots,} \alpha_q\right]^T. \tag{4.23}$$

These are the parameters that we estimate in the next section. So if we have a homogenous parameter model that fits our data it is more likely that the artery has a homogeneous structure and if we have a non homogenous parameter model that fits our data it is more likely that the artery has a non homogeneous structure however we can even have a homogeneous model to fit the data for a non homogeneous profile thus for our study we want to have both models so that we can predict or evaluate what best fits the data and investigate how far apart are our obtained estimates from their true value.

4.3.2 Deterministic Parameter Estimation

Using the above parametric model we can rewrite the statistical model in the parametric form as

$$\mathbf{y}(\mathbf{t}_j, \boldsymbol{\theta}) = \left[\mathbf{y}_u(\mathbf{t}_j, \boldsymbol{\theta})^T, \mathbf{y}_v(\mathbf{t}_j, \boldsymbol{\theta})^T\right]^T, \tag{4.24}$$

where θ is the unknown parameter and we use the distribution of the observed data to fit and obtain the value for the unknown parameter. In this case, the covariance in the measurements is expressed as

$$E\left(\left(\mathbf{y}(\mathbf{t}_j)-\mathbf{a}(\mathbf{t}_j,\boldsymbol{\theta})\right)\left(\mathbf{y}(\mathbf{t}_{j'})-\mathbf{a}(\mathbf{t}_{j'},\boldsymbol{\theta})\right)^T\right)=\Sigma\cdot\delta(j-j'), \tag{4.25}$$

where

$$\Sigma=\begin{bmatrix}\sigma_u^2\cdot I_{n_u} & 0\\ 0 & \sigma_v^2\cdot I_{n_v}\end{bmatrix},$$

Thus the distribution of the measurement vector in this case is given by

$$\mathbf{y}(\mathbf{t}_j)\sim N(\mathbf{a}(\mathbf{t}_j,\boldsymbol{\theta}),\Sigma). \tag{4.26}$$

These measurements have errors in the form of noise in them. We want to minimize the errors in these measurements, for this we consider the model predicted value

$$\hat{\mathbf{y}}(\mathbf{t}_j,\boldsymbol{\theta})=\hat{\mathbf{a}}(\mathbf{t}_j,\boldsymbol{\theta}). \tag{4.27}$$

The error in the measurements is given by the cost function. We can have different types of cost function depending on the type of the estimator. The cost function for the maximum likelihood estimator *(MLE)* is given by

$$C_{MLE}(\boldsymbol{\theta},\Sigma)=\sum_{j=1}^{p}\left(\left(\hat{\mathbf{y}}(\mathbf{t}_j,\boldsymbol{\theta})-\mathbf{y}(\mathbf{t}_j)\right)^T\Sigma^{-1}\left(\hat{\mathbf{y}}(\mathbf{t}_j,\boldsymbol{\theta})-\mathbf{y}(\mathbf{t}_j)\right)\right), \tag{4.28}$$

and we seek to obtain the parameters $\hat{\boldsymbol{\theta}}_{MLE}$ and $\hat{\Sigma}_{MLE}$ that minimizes our cost function, such that,

$$\hat{\boldsymbol{\theta}}_{MLE} = \arg\min_{\boldsymbol{\theta}} C_{MLE}\left(\boldsymbol{\theta}, \hat{\Sigma}_{MLE}\right), \tag{4.29}$$

and

$$\hat{\Sigma}_{MLE} = \frac{1}{p}\sum_{j=1}^{p}\left(\left(\hat{\mathbf{y}}\left(\mathbf{t}_j, \hat{\boldsymbol{\theta}}_{MLE}\right) - \hat{\mathbf{y}}\left(\mathbf{t}_j\right)\right)\cdot\left(\hat{\mathbf{y}}\left(\mathbf{t}_j, \hat{\boldsymbol{\theta}}_{MLE}\right) - \hat{\mathbf{y}}\left(\mathbf{t}_j\right)\right)^T\right). \tag{4.30}$$

However our covariance matrix has a simplified structure under directional independence such that

$$\Sigma^{-1} = \begin{bmatrix} \Sigma_u^{-1} \otimes I_{n_u} & 0 \\ 0 & \Sigma_v^{-1} \otimes I_{n_v} \end{bmatrix}, \tag{4.31a}$$

reduces to

$$\Sigma^{-1} = \begin{bmatrix} \frac{1}{\sigma_u^2}\cdot I_{n_u} & 0 \\ 0 & \frac{1}{\sigma_v^2}\cdot I_{n_v} \end{bmatrix}, \tag{4.31b}$$

and thus we can rewrite

$$C_{MLE}\left(\boldsymbol{\theta}, \sigma_u^2, \sigma_v^2\right) = \frac{1}{\sigma_u^2}\sum_{j=1}^{p}\left(\left\|\hat{\mathbf{y}}_u\left(\mathbf{t}_j, \boldsymbol{\theta}\right) - \mathbf{y}_u\left(\mathbf{t}_j\right)\right\|^2\right) + \frac{1}{\sigma_v^2}\sum_{j=1}^{p}\left(\left\|\hat{\mathbf{y}}_v\left(\mathbf{t}_j, \boldsymbol{\theta}\right) - \mathbf{y}_v\left(\mathbf{t}_j\right)\right\|^2\right), \tag{4.32}$$

and the parameters $\hat{\boldsymbol{\theta}}_{MLE}$, $\hat{\sigma}_{u\ MLE}^2$ and $\hat{\sigma}_{v\ MLE}^2$ that minimizes our cost function are

$$\hat{\boldsymbol{\theta}}_{MLE} = \arg\min_{\boldsymbol{\theta}} C_{MLE}\left(\boldsymbol{\theta}, \hat{\sigma}^2_{u\ MLE}, \hat{\sigma}^2_{v\ MLE}\right), \tag{4.33}$$

$$\hat{\sigma}^2_u = \frac{1}{p}\sum_{j=1}^{p}\left(\left\|\hat{\mathbf{y}}_u\left(\mathbf{t}_j, \hat{\boldsymbol{\theta}}_{MLE}\right) - \mathbf{y}_u\left(\mathbf{t}_j\right)\right\|^2\right), \tag{4.34}$$

and

$$\hat{\sigma}^2_v = \frac{1}{p}\sum_{j=1}^{p}\left(\left\|\hat{\mathbf{y}}_v\left(\mathbf{t}_j, \hat{\boldsymbol{\theta}}_{MLE}\right) - \mathbf{y}_v\left(\mathbf{t}_j\right)\right\|^2\right). \tag{4.35}$$

Similarly the least squares *(LS)* cost function can be written as

$$C_{LS}(\boldsymbol{\theta}) = \sum_{j=1}^{p}\left\|\hat{\mathbf{y}}\left(\mathbf{t}_j, \boldsymbol{\theta}\right) - \mathbf{y}\left(\mathbf{t}_j\right)\right\|^2, \tag{4.36}$$

and we seek to obtain the parameter $\hat{\boldsymbol{\theta}}_{LS}$ that minimizes the cost function such that

$$\hat{\boldsymbol{\theta}}_{LS} = \arg\min_{\boldsymbol{\theta}} C_{LS}(\boldsymbol{\theta}) \tag{4.37}$$

As our measurement vector is a combination of measurements of velocity and deformation measurements that have different noise variances, we consider to put weights A and B on our measurements. These weights are inversely proportional to the variances of these measurements and are chosen to determine the importance of one measurement over the other and how much the each observation influences the final estimates. Thus we have,

$$C_{LS}(\boldsymbol{\theta}) = \left(A \cdot \sum_{j=1}^{p} \left\| \hat{\mathbf{y}}_{v}(\mathbf{t}_j, \boldsymbol{\theta}) - \mathbf{y}_{v}(\mathbf{t}_j, \boldsymbol{\theta}) \right\|^2 + B \cdot \sum_{j=1}^{p} \left\| \hat{\mathbf{y}}_{u}(\mathbf{t}_j, \boldsymbol{\theta}) - \mathbf{y}_{u}(\mathbf{t}_j, \boldsymbol{\theta}) \right\|^2 \right). \tag{4.38}$$

We seek to obtain the parameter $\hat{\boldsymbol{\theta}}$ that minimizes our cost function.

$$\hat{\boldsymbol{\theta}}_{LS} = \arg\min_{\boldsymbol{\theta}} \left(A \cdot \sum_{j=1}^{p} \left\| \hat{\mathbf{y}}_{v}(\mathbf{t}_j, \boldsymbol{\theta}) - \mathbf{y}_{v}(\mathbf{t}_j, \boldsymbol{\theta}) \right\|^2 + B \cdot \sum_{j=1}^{p} \left\| \hat{\mathbf{y}}_{u}(\mathbf{t}_j, \boldsymbol{\theta}) - \mathbf{y}_{u}(\mathbf{t}_j, \boldsymbol{\theta}) \right\|^2 \right), \tag{4.39}$$

and estimate of the variances in the measurements of velocity and deformation i.e.

$$\hat{\sigma}_{u}^{2} = \frac{1}{p} \sum_{j=1}^{p} \left\| \hat{\mathbf{y}}_{u}\left(\mathbf{t}_j, \hat{\boldsymbol{\theta}}\right) - \mathbf{y}_{u}(\mathbf{t}_j) \right\|^2, \tag{4.40a}$$

$$\hat{\sigma}_{v}^{2} = \frac{1}{p} \sum_{j=1}^{p} \left\| \hat{\mathbf{y}}_{v}\left(\mathbf{t}_j, \hat{\boldsymbol{\theta}}\right) - \mathbf{y}_{v}(\mathbf{t}_j) \right\|^2. \tag{4.40b}$$

The weighted least squares estimation approach tries to minimize the residual noise by attempting to minimize the squared difference between the model generated measurement data $\hat{\mathbf{y}}(\mathbf{t}_j, \boldsymbol{\theta})$ and the noisy observation measurement data $\mathbf{y}(\mathbf{t}_j, \boldsymbol{\theta})$. The noisy observation data depends on the unknown parameter $\boldsymbol{\theta}$ that we wish to estimate. The least squares estimator *(LSE)* of $\boldsymbol{\theta}$, where $\hat{\boldsymbol{\theta}}$ chooses that value of $\boldsymbol{\theta}$ that makes $\hat{\mathbf{y}}(\mathbf{t}_j, \boldsymbol{\theta})$ closest to the observation measurement data $\mathbf{y}(\mathbf{t}_j, \boldsymbol{\theta})$. Thus to minimize the cost function we take the partial derivative with respect to parameter $\boldsymbol{\theta}$ and equate it to zero.

$$\frac{\partial C_{LS}(\boldsymbol{\theta})}{\partial \boldsymbol{\theta}} = \frac{\partial}{\partial \boldsymbol{\theta}}\left(A \cdot \sum_{j=1}^{p} \left\| \hat{\mathbf{y}}_v(\mathbf{t}_j, \boldsymbol{\theta}) - \mathbf{y}_v(\mathbf{t}_j, \boldsymbol{\theta}) \right\|^2 + B \cdot \sum_{j=1}^{p} \left\| \hat{\mathbf{y}}_u(\mathbf{t}_j, \boldsymbol{\theta}) - \mathbf{y}_u(\mathbf{t}_j, \boldsymbol{\theta}) \right\|^2 \right) = 0, \quad (4.41)$$

This derivative is not available in the analytical form as it is derivative of a function obtained from the of the *Comsol* forward model. There are various numerical techniques that can be used to minimize $C_{LS}(\boldsymbol{\theta})$. The speed and accuracy of the algorithm depends on the choice of the search algorithm and how close the initial guess is from the true value of the parameter. We will discuss the search method used and the performance evaluation of the proposed algorithm by computing the mean square error in the measurement and the means square error in the estimate in the next chapter.

4.3.3 Stochastic parameter model

From our measurement model we have,

$$\mathbf{y}(\mathbf{t}_j) = (\mathbf{a}(\mathbf{t}_j, \boldsymbol{\theta}) + \boldsymbol{\varepsilon}(\mathbf{t}_j))^T \tag{4.42}$$

where we can have an apriori knowledge about $\boldsymbol{\theta}$ from the experimental studies about the elasticity of the arteries [Fung, 1993]. Thus we can have $\boldsymbol{\theta}$ to be viewed as a random variable coming from a known distribution $f_\theta(\boldsymbol{\theta}, \mathbf{t}_j)$. In this case the assumption that $\mathbf{y}(\mathbf{t}_j)$ is Gaussian no longer holds as because the distribution of the transfer vector $\mathbf{a}(\mathbf{t}_j, \boldsymbol{\theta})$ is unknown because of the random nature of the stochastic parameter. Considering that $\mathbf{a}(\mathbf{t}_j, \boldsymbol{\theta})$ and $\boldsymbol{\varepsilon}(\mathbf{t}_j)$ are random variables the distribution of $\mathbf{y}(\mathbf{t}_j)$ is obtained as a convolution of the random variables thus,

$$f_y(\mathbf{t}_j) = f_\theta(\boldsymbol{\theta}, \mathbf{t}_j) \otimes f_\varepsilon(\mathbf{t}_j, \Sigma), \tag{4.42}$$

where $f_y(\mathbf{t}_j)$ is the distribution of $\mathbf{y}(\mathbf{t}_j)$, $f_\theta(\boldsymbol{\theta}, \mathbf{t}_j)$ is the distribution of $\mathbf{a}(\mathbf{t}_j, \boldsymbol{\theta})$ and $f_\varepsilon(\mathbf{t}_j, \Sigma)$ is the distribution of $\boldsymbol{\varepsilon}(\mathbf{t}_j)$. As this is a convolution of two distributions which is no longer Gaussian we have a more complex distribution that can be computed numerically. Thus we can have $\boldsymbol{\theta}$ to be viewed as a random variable coming from a known distribution $f_\theta(\boldsymbol{\theta}, \mathbf{t}_j)$. The distribution of $\boldsymbol{\theta}$ plays a vital role in the estimation and any prior knowledge about the parameter distribution can provide a better guess of the parameter $\boldsymbol{\theta}$. The distribution of measurement $\mathbf{y}_i$ is interpreted as a conditional

distribution $f_y(\mathbf{y} \mid \boldsymbol{\theta})$. Here the problem is to estimate the value of $\boldsymbol{\theta}$ for the random variable $\boldsymbol{\theta}$. Thus the problem of estimation is changed to that of prediction. To solve such a problem of *Bayesian Estimation,* we assume that no observations are available that is, the available information is now the *prior* density $f_\theta(\boldsymbol{\theta}, \mathbf{t}_j)$ of $\boldsymbol{\theta}$ which we assume known, and our problem is to find a constant $\hat{\boldsymbol{\theta}}$ close in some sense to the unknown parameter $\boldsymbol{\theta}$. The $\hat{\boldsymbol{\theta}}$ is estimated in this case as

$$\hat{\boldsymbol{\theta}} = E\{\boldsymbol{\theta} \mid \mathbf{y}\} = \int_{-\infty}^{\infty} \boldsymbol{\theta} \cdot f_\theta(\boldsymbol{\theta} \mid \mathbf{y}) d\boldsymbol{\theta}, \tag{4.43}$$

where

$$f_\theta(\boldsymbol{\theta} \mid \mathbf{y}) = \frac{f_\theta(\mathbf{y} \mid \boldsymbol{\theta})}{f_y(\mathbf{t}_j)} \cdot f_\theta(\boldsymbol{\theta}, \mathbf{t}_j). \tag{4.44}$$

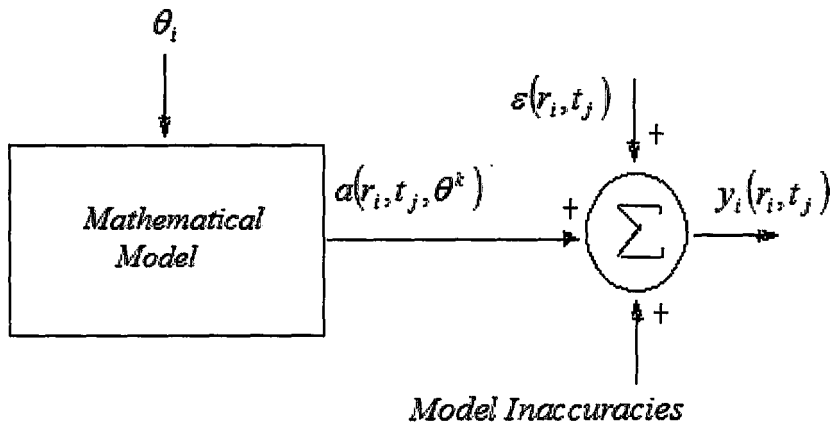

Fig. 4.2 Measurement Model. [Kay 1993]

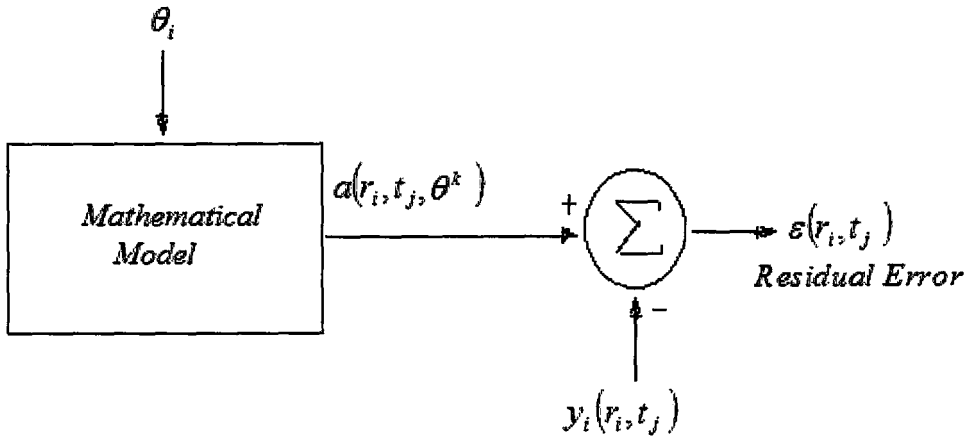

Fig. 4.3 Least Squares Approach. [Kay, 1993]

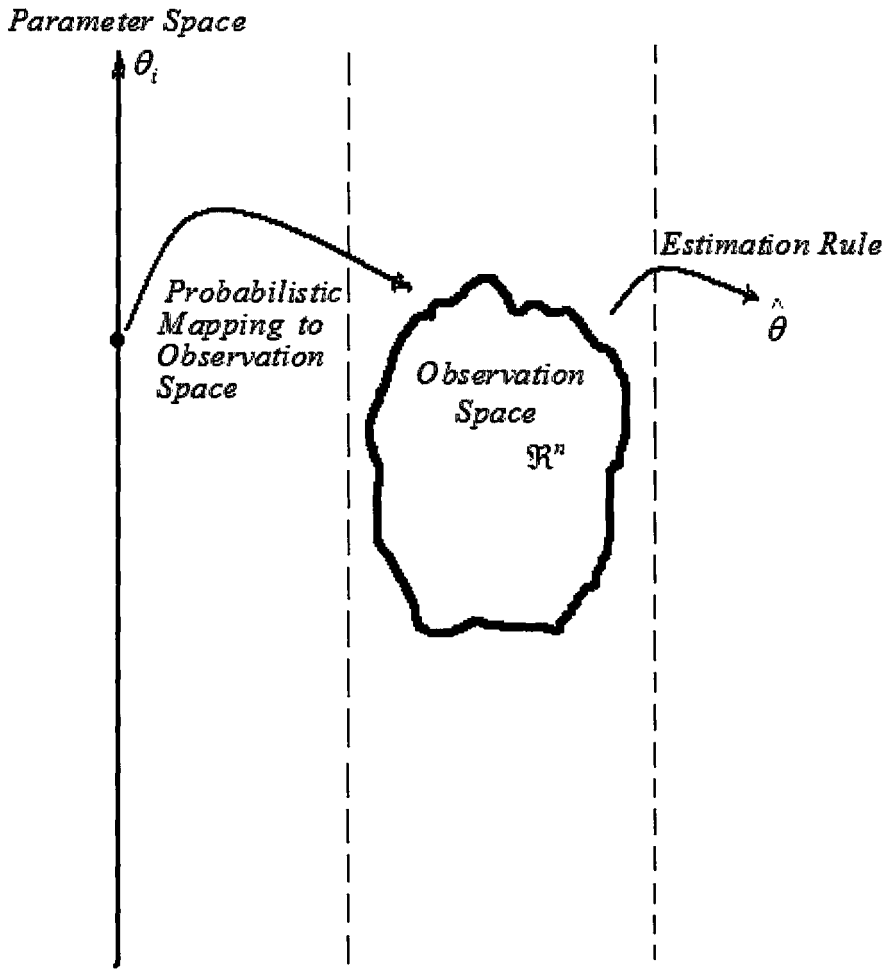

Fig. 4.4 Estimation Model. [Van Trees, 2001]

Chapter 5

Numerical Examples

In this Chapter, we evaluate the applicability of the statistical model proposed in the previous chapter. We use numerical examples to demonstrate the performance measures of our estimators and then we discuss our numerical results obtained by implementation of the estimation algorithm in *MATLAB*.

5.1 Performance Measure

To perform statistical analysis on our measurements, we import the measurement vector from *Comsol* to *Matlab*. The velocity and deformation measurements consists noise in them as discussed in Chapter 4. Let σ_u^2 and σ_v^2 represent the variance (power) of noise in the deformation and velocity measurement vectors $\mathbf{y}_u$ and $\mathbf{y}_v$ such that,

$$\hat{\sigma_u^2} = \frac{1}{p}\sum_{j=1}^{p}\left\|\hat{\mathbf{y}}_u(\mathbf{t}_j,\boldsymbol{\theta}) - \mathbf{y}_u(\mathbf{t}_j)\right\|^2, \tag{5.1}$$

and

$$\hat{\sigma_v^2} = \frac{1}{p}\sum_{j=1}^{p}\left\|\hat{\mathbf{y}}_v(\mathbf{t}_j,\boldsymbol{\theta}) - \mathbf{y}_v(\mathbf{t}_j)\right\|^2, \tag{5.2}$$

then the signal to noise ratio, (*SNR*) in dB for the deformation measurements is defined as,

$$SNR_u = 10\log\left(\frac{\sum\|\mathbf{y}_u\|_2^2}{\sigma_u^2}\right), \tag{5.3}$$

and the signal to noise ratio, (*SNR*) in dB for the velocity measurements is defined as,

$$SNR_v = 10\log\left(\frac{\sum\|\mathbf{y}_v\|_2^2}{\sigma_v^2}\right). \tag{5.4}$$

To measure the performance of our estimator, we compute the mean square error (*MSE*) where the amount by which an estimator $\hat{\boldsymbol{\theta}}$ differs from its true value is given by,

$$MSE(\boldsymbol{\theta}) = \frac{1}{\|\boldsymbol{\theta}\|^2}\cdot\left\|\left(\hat{\boldsymbol{\theta}}-\boldsymbol{\theta}\right)\right\|^2, \tag{5.5}$$

The magnitude of *MSE* allows us to compute the performance of our estimation.

We also compute the *MSE* of the measurement vector, which can be termed as 'curve fitting' so that we can determine weather the analytical model fits the measured data. This allows us to determine how much modeling error was present when we simulate the measurements as compared to the analytical model. The mean squared error between the model $\hat{\mathbf{y}}$, and the measurements $\mathbf{y}$ is given by

$$MSE(\mathbf{y}) = \frac{1}{p \cdot (n_v + n_u)} \cdot \sum_{j=1}^{p} \left\| \left(\hat{\mathbf{y}}(\mathbf{t}_j, \boldsymbol{\theta}) - \mathbf{y}(\mathbf{t}_j) \right) \right\|^2 . \tag{5.6}$$

5.2 Numerical Examples

To study how the noise in the measurements affects our ability to estimate the parameters, we formulate numerical examples in which the elasticity of the artery is considered to have a non homogeneous profile. In this case, we consider elasticity being a single spatially varying exponential basis function; and that this can easily be extended to a set of multiple spatial basis functions that model the change in elasticity. Here we simulate our measurements considering

$$G = (G_s - G_0) \cdot e^{\{-\alpha \cdot [(x-x_0)^2 + (y-y_0)^2 + (z-z_0)^2]^2\}} + G_0 , \tag{5.7}$$

where $x_0=1.5$, $y_0=0$, $z_0=6.5$ are considered to be known, α is the decay constant, and G_s-G_0 represents the range of elasticity. Here we consider two cases

1. Estimating a single unknown parameter, shear modulus G_s.
2. Estimating two unknown parameters, shear modulus G_s, and the decay constant α.

In all the examples unless otherwise stated, we assume the shear modulus G_0= *6e6 Pa*, deformation $SNR_u=15dB$, velocity $SNR_v=15dB$, number of deformation spatial points $n_u=250$ and the number of velocity spatial points $n_v=1000$.

In the first case of single parameter estimation, where we consider same noise to be present in a combined measurement vector of velocity and deformation measurements. Here we fix the decay constant $\alpha = 2$ and estimate the shear modulus G_s.

We extend this numerical example to a case of two parameter estimation, where we consider different noise in velocity and deformation measurements. In this case, to study the effect of different noise variances in deformation and velocity measurements we consider one example where we fix the number of deformation measurement points n, the number of velocity measurement points n_v, the *SNR* in velocity measurements and vary the *SNR* in deformation measurements. Further, we consider another example where we fix the number of deformation points n_u, the number of velocity measurement points n_v, the *SNR* in deformation measurements and vary the *SNR* in velocity measurements.

In the Chapter 2, we described the limitations on the spatial resolution for obtaining our measurements. When we design our estimator it is important that we take into consideration the number of measurement points. To study the effect of the number of measurement points on performance of our estimator we consider a numerical example where we fix the number of deformation points n_u, and the noise in the velocity and deformation measurements and vary the number of velocity measurement points n_v Further, we consider one more numerical example where we fix the number of velocity points n_v, and the noise in the velocity and deformation measurements and vary the number of deformation points n_u. Here elasticity being a function of single linear spatial basis function of two unknown parameters; we estimate the shear modulus G_s and the

decay constant α, of the above mentioned basis function. Thus the parameter $\boldsymbol{\theta}$ in this case, is a vector of two parameters G_s and α.

This example can further straight forwardly be simplified to a case of homogenous elasticity profile where we treat the shear modulus to be a constant G.

5.3 Numerical Results

In this section, we discuss the plots obtained for our numerical examples. We further evaluate the performance of the estimation algorithm by making some observations regarding the plots.

We use the *fminsearch* and *lsqnonlin* commands in Matlab to minimize the least squares costfunction. The *fminsearch* command minimizes the least squares function by using the Nelder mead simplex search method [Neadler, Mead, 1965] and the *lsqnonlin* command performs nonlinear minimization using the trust region method [Coleman, Li, 1996]. In both the cases we choose an initial starting guess for the estimate which has a significant effect on the minimization.

For clarity of presentation we will refer the $MSE(\boldsymbol{\theta})$ as mean square error and MSE($\mathbf{y}$) as goodness of fit. For the first numerical example where we considered estimation of one parameter the shear modulus of the artery G_s, the Fig. 5.1 shows the mean square error in the estimate versus the signal to noise ratio in the measurements, For the second numerical example we considered the estimation of two parameters, the shear modulus of

the artery G_s and the decay constant in the basis function α. The Fig. 5.3a and 5.3b shows the mean square error in the estimate of parameters θ_1 and θ_2 versus the signal to noise ratio in the velocity measurements considering fixed noise in the deformation measurements. The Fig. 5.4a and 5.4b shows the means square error in the estimate of parameters θ_1 and θ_2 versus the signal to noise ratio in the deformation measurements considering fixed noise in the velocity measurements. As expected the mean square error decreases significantly as the *SNR* increases which means in order to estimate our parameters accurately we need less noise in our measurements. The Fig. 5.5a and Fig. 5.5b we plot the mean square error in the estimate of parameters θ_1 and θ_2 vs. the number of velocity measurement and in Fig. 5.6a and Fig. 5.6b. We plot the mean square error in the estimate of parameters θ_1 and θ_2 vs. the number of deformation measurements. Here we see that we get a significant decay in the mean square error as the number of velocity points increases, however we do not see the same when we move form *500* to *1000* deformation points thus it is more beneficial to increase the velocity points for our estimation.

We plot the goodness of fit as a function of *SNR* (dB) and the parameter θ to see how well the model data fits the measurement data. For Fig. 5.2 we consider θ to be a single parameter, we can see the plot of goodness of fit plotted against the signal to noise ratio in the measurements and here we also include the dependence on the parameter θ because we want to study the performance of the algorithm for both the different values of parameters. We see that it is a little sensitive to the parameter for low values of *SNR*

however for larger values it does not change much in general it does not change much with the parameter. Further we consider the parameter $\boldsymbol{\theta}$ to be a vector of two parameters $\boldsymbol{\theta}_1$ and $\boldsymbol{\theta}_2$. In Fig. 5.7-Fig. 5.9, we consider constant number of velocity measurements with fixed noise in it and vary the deformation measurements for different SNR and plot against parameter $\boldsymbol{\theta}_1$. We plot the same against parameter $\boldsymbol{\theta}_2$ in Fig. 5.13-Fig. 5.15. For Fig. 5.10-Fig. 5.12, we consider constant number of deformation measurements with fixed noise in it and vary the velocity measurements for different SNR and plot against parameter $\boldsymbol{\theta}_1$ and we plot the same against parameter $\boldsymbol{\theta}_2$ in Fig. 5.16-Fig. 5.18. We observe that for the least squares estimation, the parameters are identifiable with our estimation algorithm. When we try to estimate a single parameter as in Fig 5.1, or two parameters as in Fig 5.3, Fig 5.4 the $MSE(\hat{\boldsymbol{\theta}})$ decreases as the SNR in the measurement increases thus we infer that we can have a better estimates for our parameters if we have less noise in our measurements. Further, we see in Fig 5.5, that with the increase in the number of measurement points of velocity $MSE(\hat{\boldsymbol{\theta}})$ decreases and in Fig 5.6, it can be seen that with the increase in the number of deformation measurement points the $MSE(\hat{\boldsymbol{\theta}})$ decreases. Thus we infer from this that if we have more number of measurements available for our estimation for both velocity and deformation we can minimize the error in our estimation. We observe in Fig 5.2 and Fig 5.7-Fig 5.18, that when comparing the goodness of fit while estimating either one parameter or two parameters, that the fit is more sensitive to the data for higher *SNR* and more number of velocity and deformation measurements.

Thus we infer from the above study that the parameters are identifiable. The accuracy of estimation and the efficiency in computational cost can be increased with the choice of a better estimation technique which is a subject of further study.

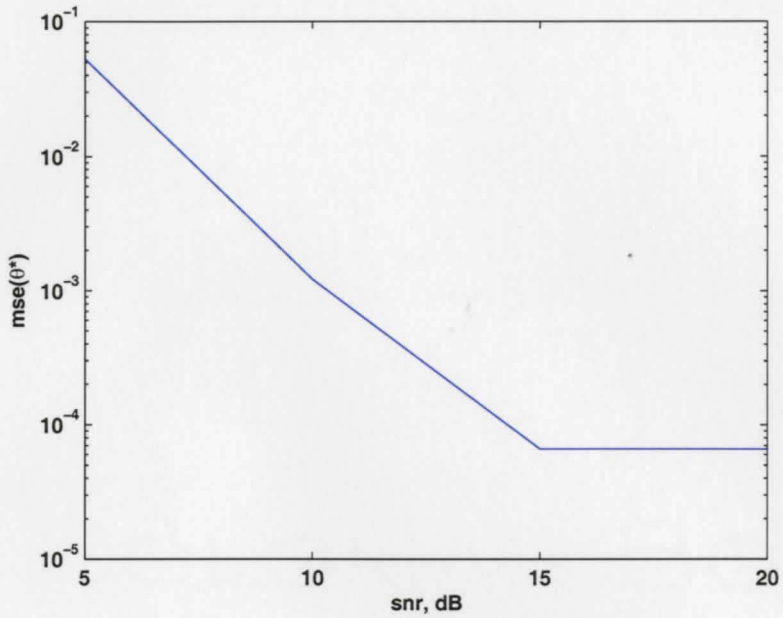

Fig. 5.1 MSE $(\hat{\theta})$ vs. SNR for single parameter estimation.

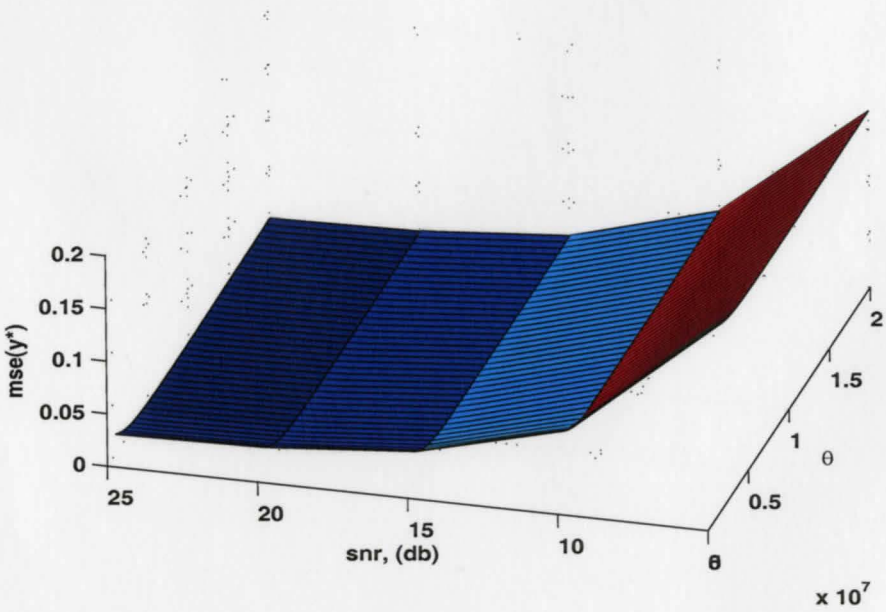

Fig. 5.2 Goodness of fit vs. SNR for one parameter estimation.

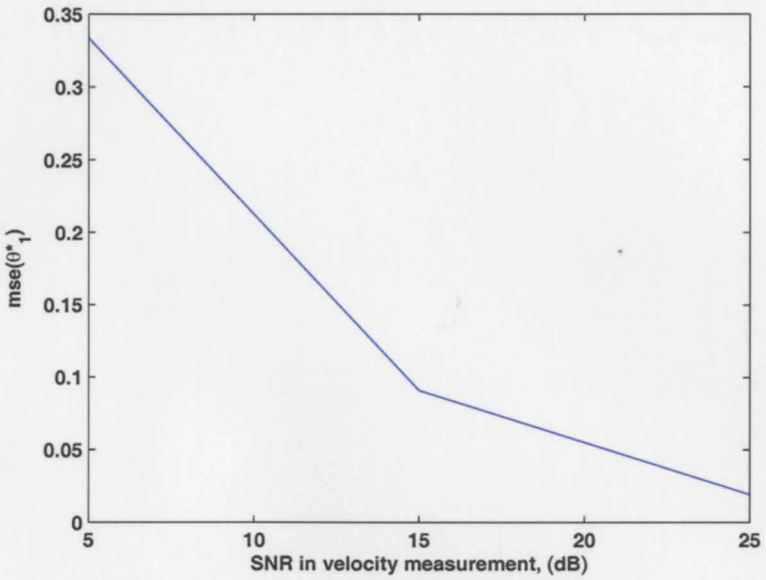

Fig. 5.3a MSE $(\hat{\theta}_1)$ vs. SNR for velocity measurements.

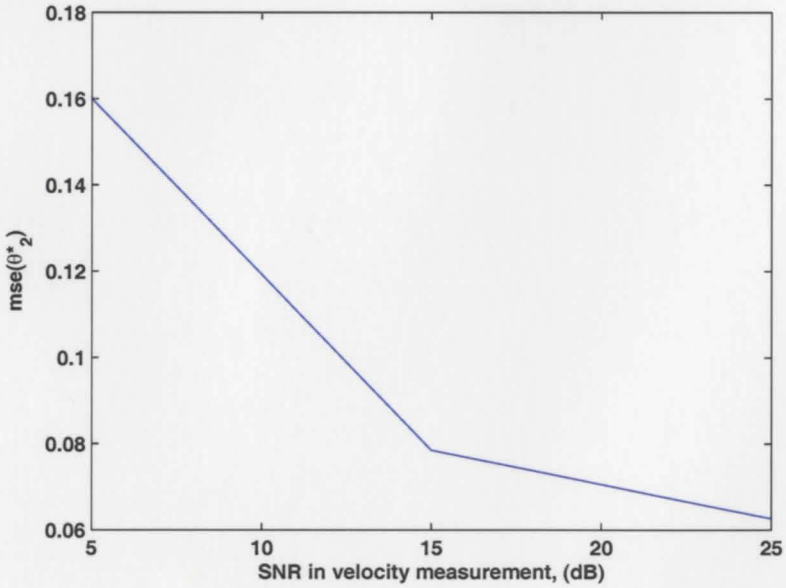

Fig. 5.3b MSE $(\hat{\theta}_2)$ vs. SNR for velocity measurements.

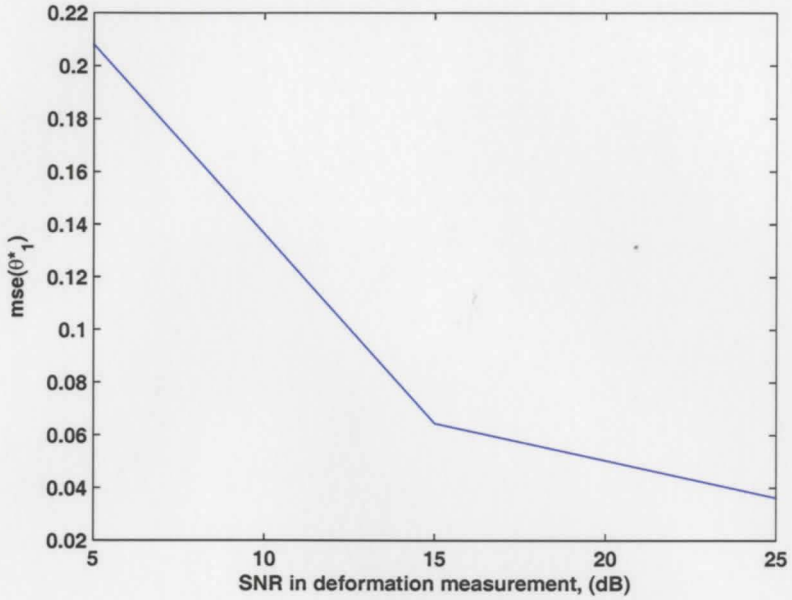

Fig. 5.4a MSE $(\hat{\theta}_1)$ vs. SNR for deformation measurements.

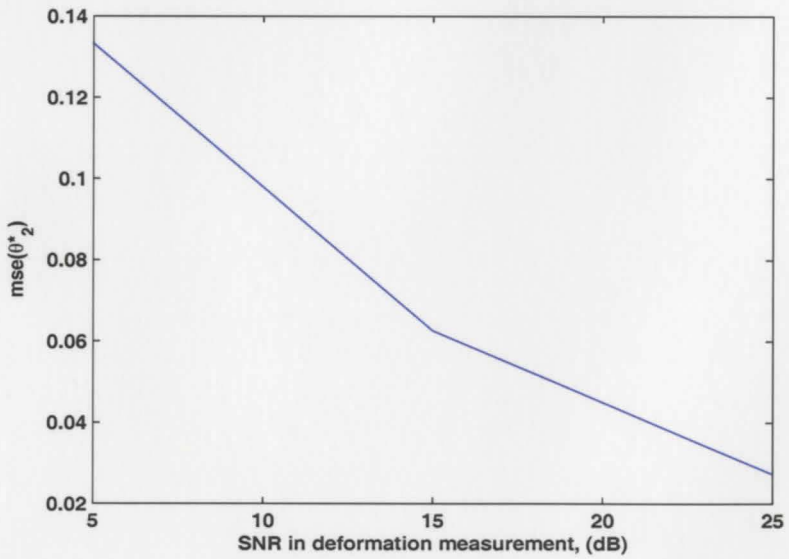

Fig. 5.4b MSE $(\hat{\theta}_2)$ vs. SNR for deformation measurements.

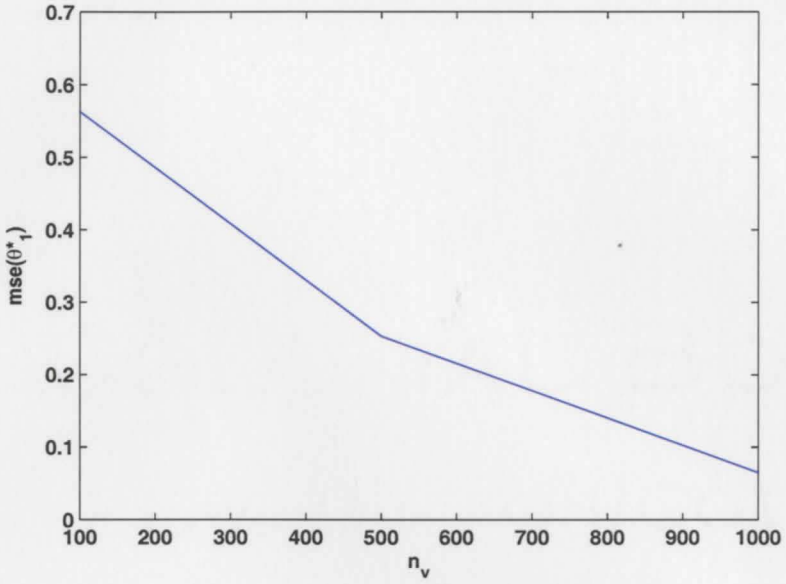

Fig. 5.5a MSE $(\hat{\theta}_1)$ vs. number of velocity measurements.

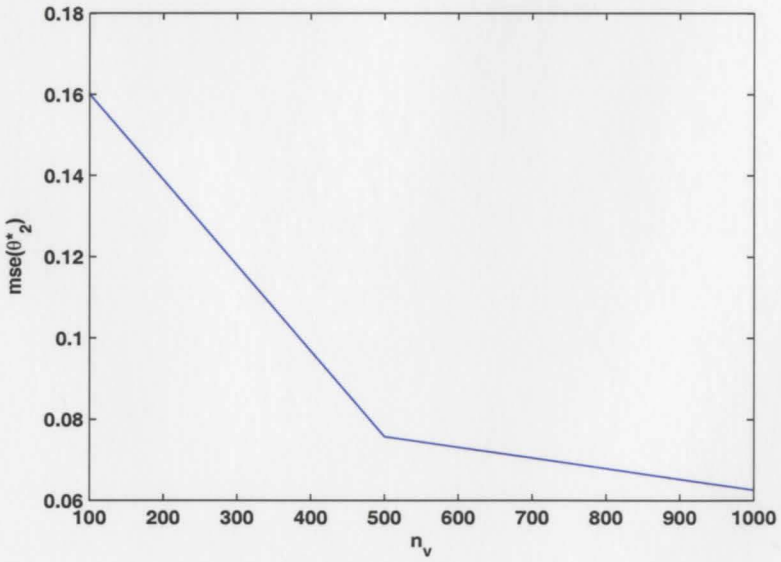

Fig. 5.5b MSE $(\hat{\theta}_2)$ vs. number of velocity measurements.

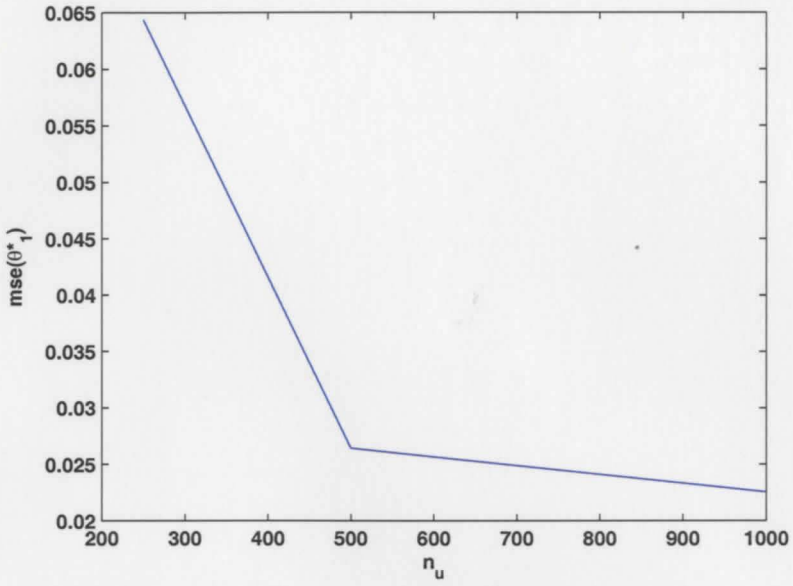

Fig. 5.6a MSE $(\hat{\theta}_1)$ vs. number of deformation measurements.

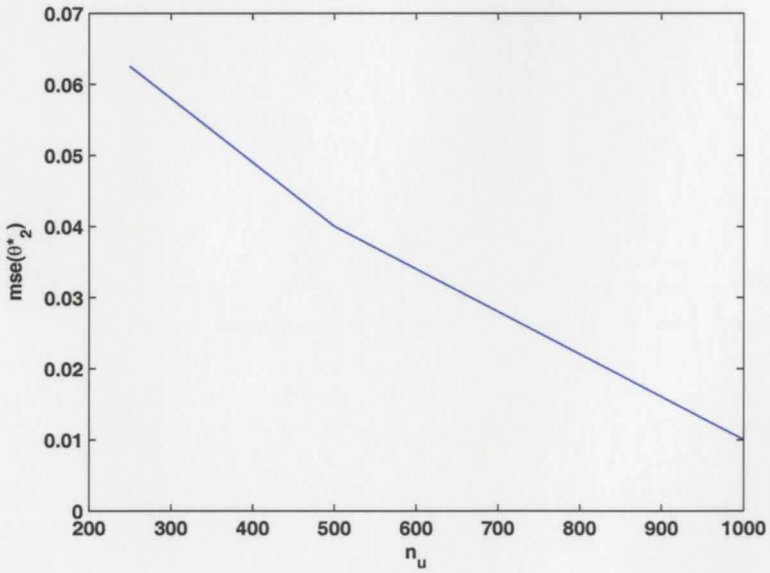

Fig. 5.6b MSE $(\hat{\theta}_2)$ vs. number of deformation measurements.

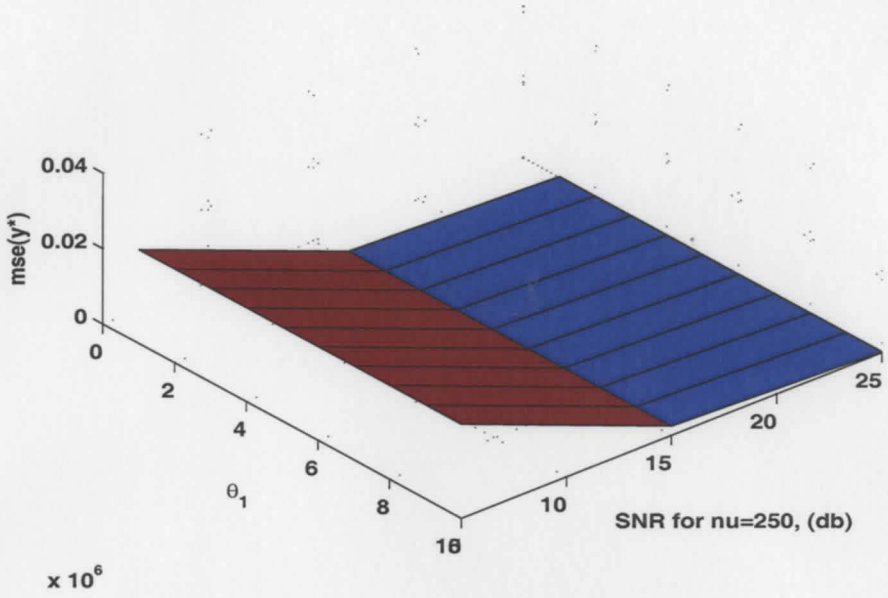

Fig. 5.7 Goodness of fit vs. SNR for 250 deformation points.

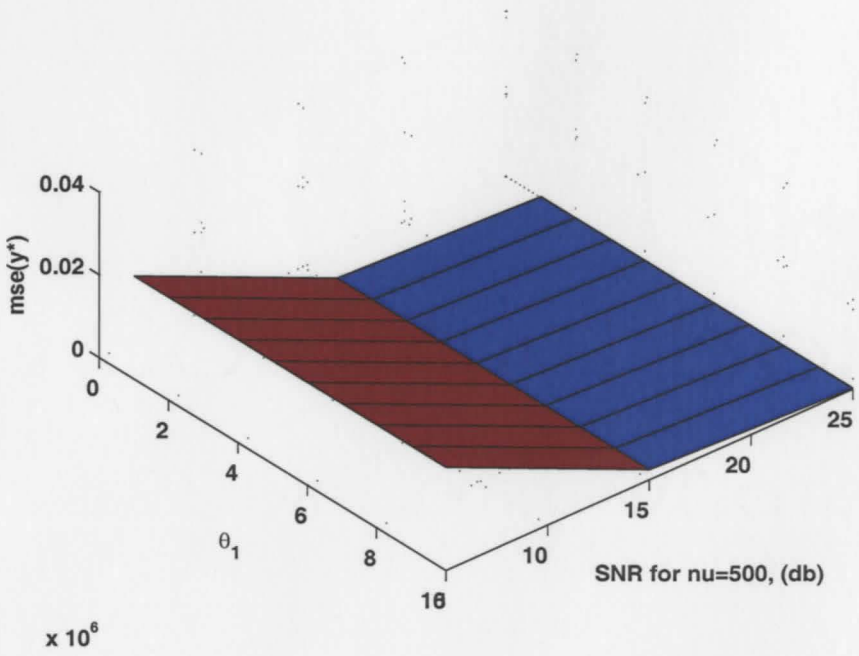

Fig. 5.8 Goodness of fit vs. SNR for 500 deformation points.

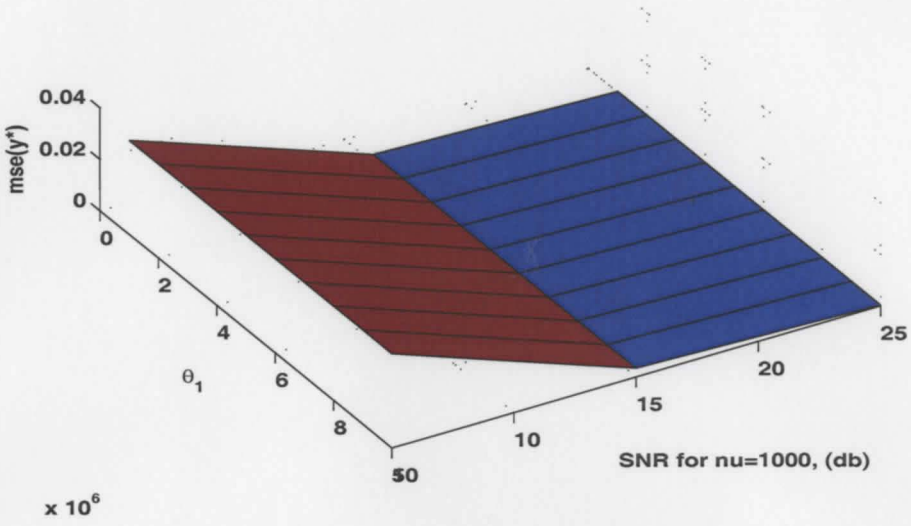

Fig. 5.9 Goodness of fit vs. SNR for 1000 deformation points.

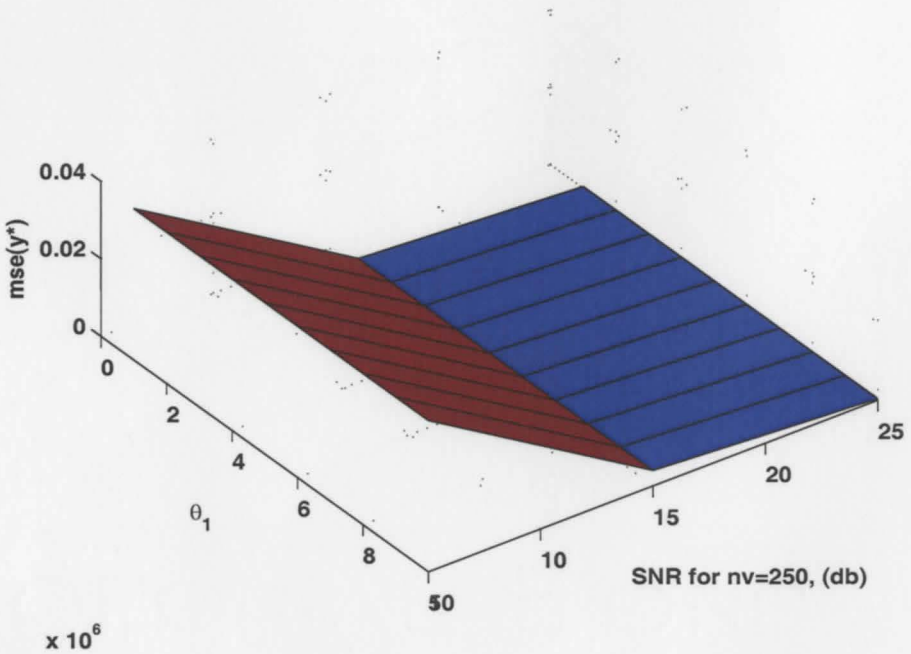

Fig. 5.10 Goodness of fit vs. SNR for 250 velocity points.

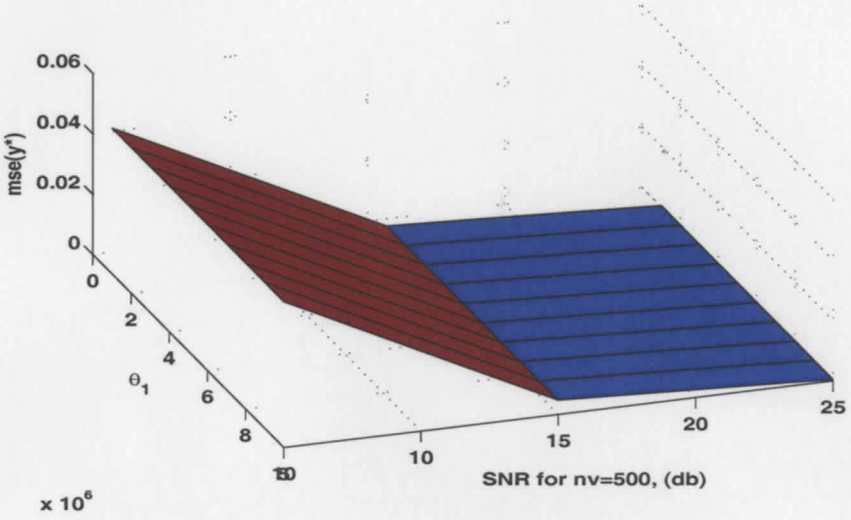

Fig. 5.11 Goodness of fit vs. SNR for 500 velocity points.

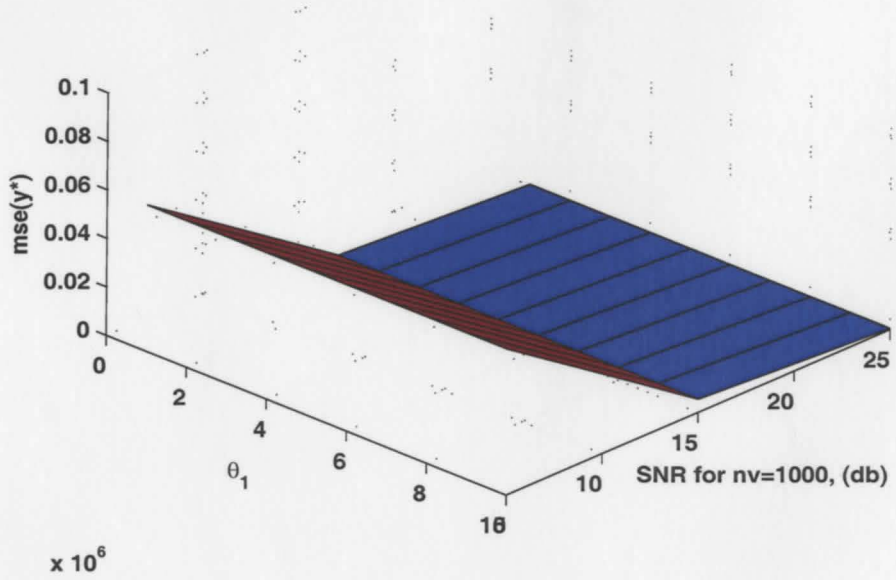

Fig. 5.12 Goodness of fit vs. SNR for 1000 velocity points.

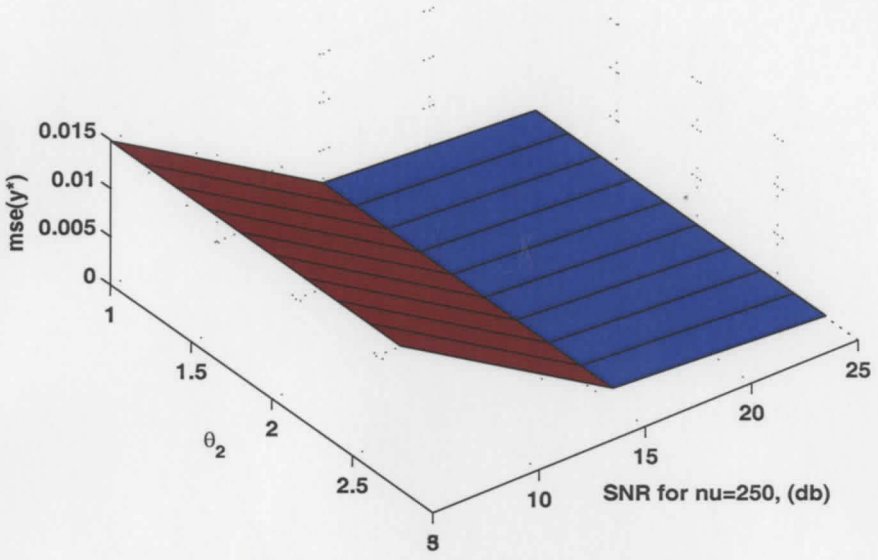

Fig. 5.13 Goodness of fit vs. SNR for 250 deformation points.

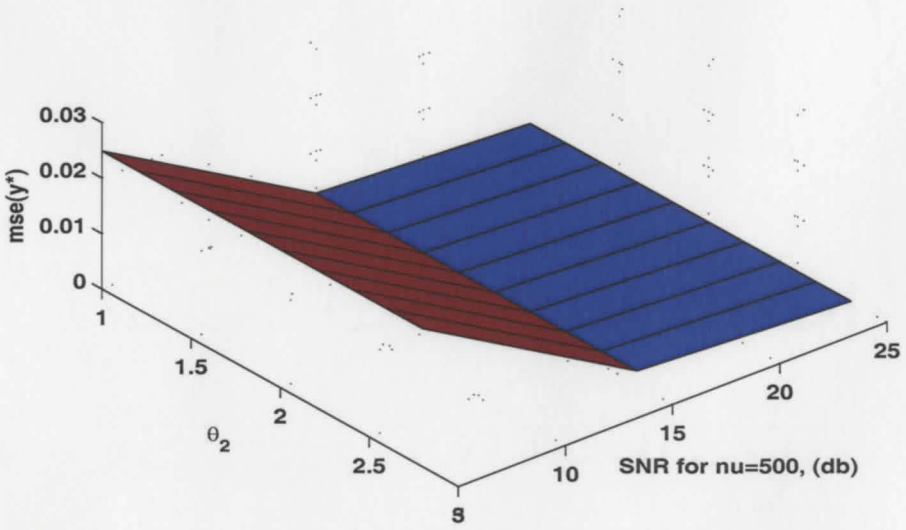

Fig. 5.14 Goodness of fit vs. SNR for 500 deformation points.

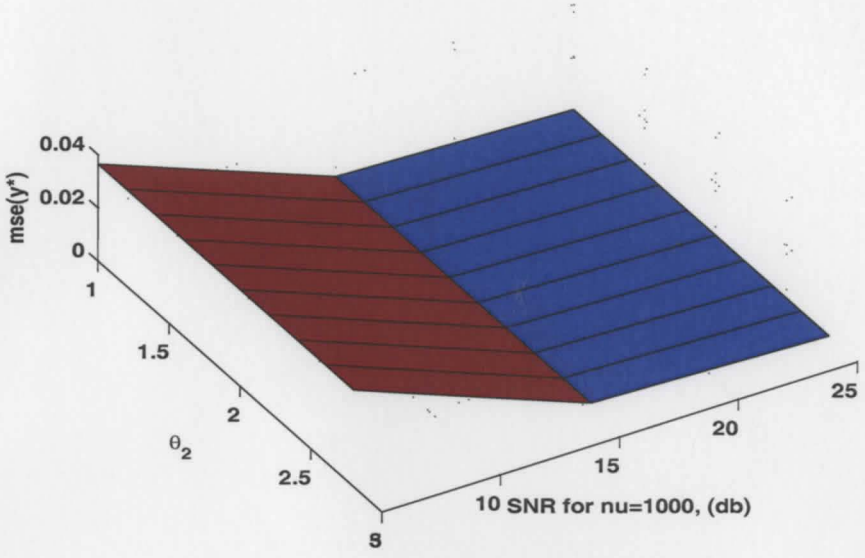

Fig. 5.15 Goodness of fit vs. SNR for 1000 deformation points.

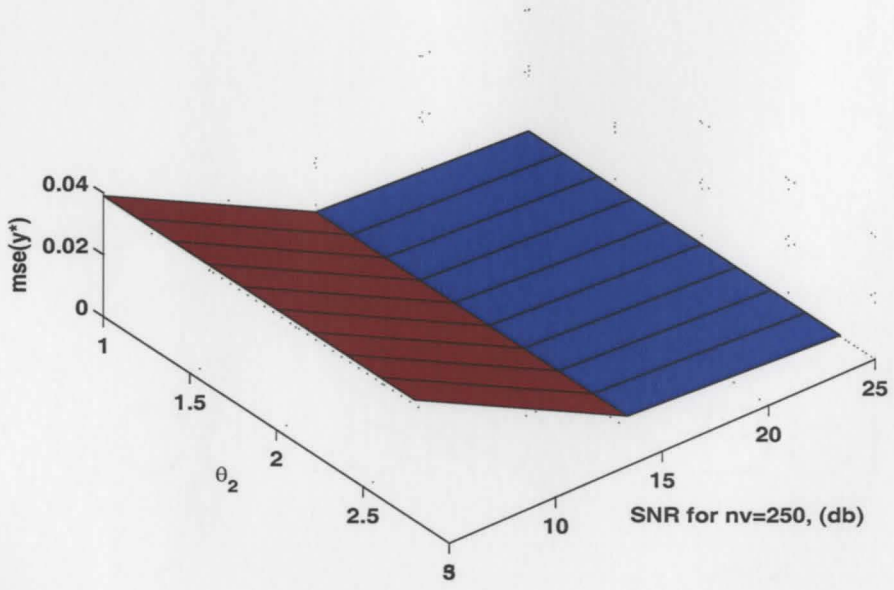

Fig. 5.16 Goodness of fit vs. SNR for 250 velocity points.

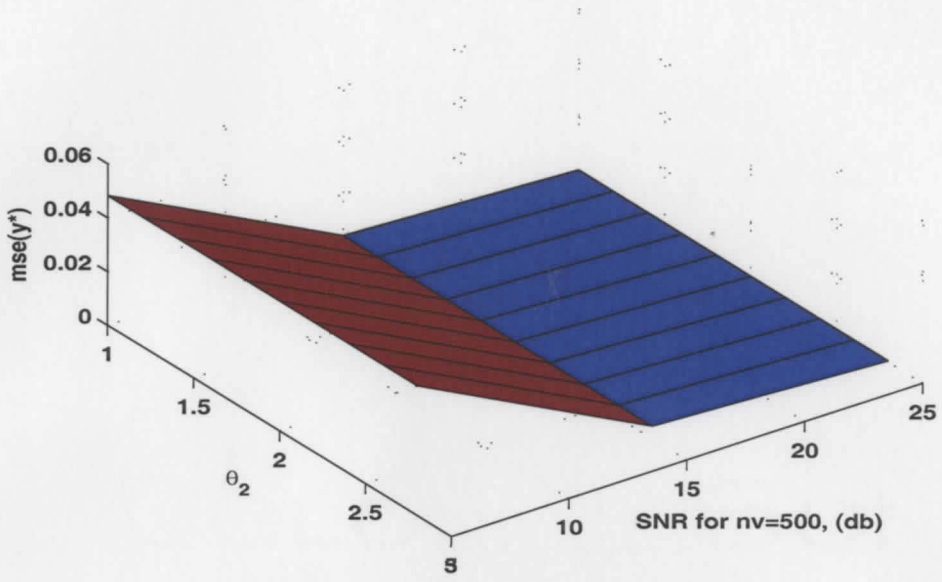

Fig. 5.17 Goodness of fit vs. SNR for 500 velocity points.

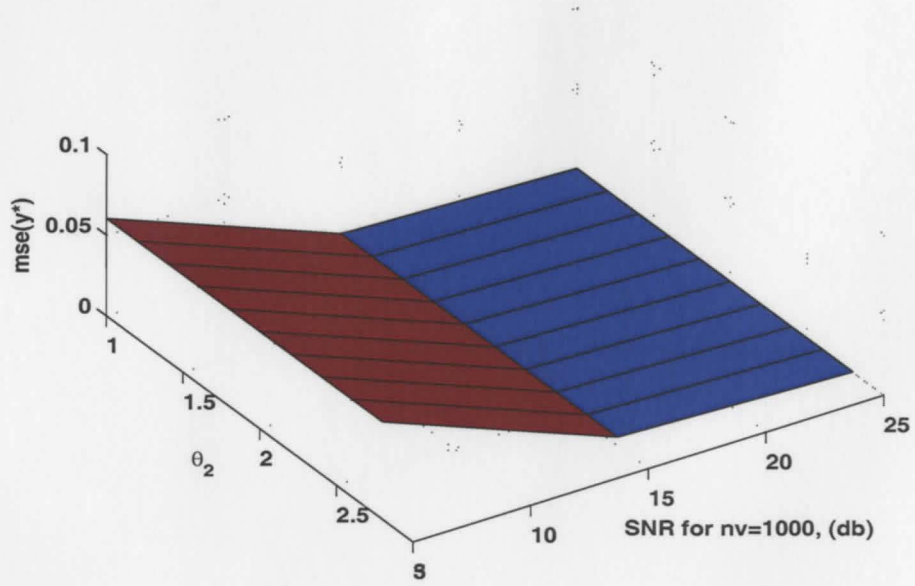

Fig. 5.18 Goodness of fit vs. SNR for 1000 velocity points.

Chapter 6

Conclusion and Future work

In this Chapter, we present the conclusion of our work and discuss some future directions in which the study can be extended.

6.1 Conclusion

In this thesis, we developed a forward mathematical model to simulate the flow of blood through the artery in normal healthy condition and in conditions of some pathological abnormality such as atherosclerosis. We used the three dimensional Navier-Stokes equation to model the blood flow, the deformation in the artery and cardiac muscle was computed considering the artery to be a hyperelastic material. Further, we proposed inverse computational model for the estimating the elasticity profile of the arterial wall to locate the region of atherosclerosis using the velocity and deformation measurements. We demonstrated how the coefficients which represented the atherosclerosis can be estimated by minimizing the error between the measurement data set and the estimator model data set. We demonstrated this applicability by using numerical examples and analyzed the performance of our estimator by computing the mean square error. It can be seen from the results of our numerical examples that there are particular threshold associated with the signal to noise ratio and number of measurement points that can be useful in the

design of experiments. We thus reached to a conclusion that with our estimation model the parameters are identifiable.

6.2 Future work

Future possibilities of this work include developing the forward mathematical model for realistic measurements obtained from experiments such as Doppler ultrasound method and Tagged MRI method. For our analysis, we confined ourselves by considering the medium to be isotropic this can be extended to anisotropic medium. We also considered the blood flow to be laminar however it is very likely that there is presence of turbulence in the regions of atherosclerosis, the study can be extended to the modeling of blood flow in presence of turbulence.

For the inverse model, we can develop better estimation techniques to accurately localize the region of atherosclerosis. We can compare the performance of weighted least squares estimator to other estimators like the maximum likelihood estimator. We can even perform variance analysis using Cramer Rao lower bound. The study was done considering the parameters to be deterministic; this can be extended to case where the parameters are stochastic in nature. From a physiological point of view, we considered estimating the region of hardening in the artery; however this model can easily be extended to estimating a wide range of different parameters like the pressure drop that governs the blood flow, the viscosity of the blood, the poisons ratio etc.

REFERENCES

[Papoulis, 2002] - Papuolis A and Pillai S U, *Probability Random Variable and Stochastic Process,* Tata McGraw Hill, 4thEdition, 2002.

[Landau, 1970] - Landau and Lifshitz, *Theory of Elasticity*, 2nd English edition, Pergamon Press, 1970.

[Panton, 1996] - Panton R L, *Incompressible Flow*, Wiley-Interscience Publication, 2nd Edition, 1996.

[Kundu, 2004] - Kundu P K and Cohen I M, *Fluid Mechanics*, Elsevier Press, 3rd Edition, 2004.

[Fung, 1993] - Fung Y C, *Biomechanics-Mechanical properties of living tissues*, Springer-Verlag Publisher, 2nd Edition, 1993.

[Fung, 1990] - Fung Y C, *Biomechanics-Motion, Flow, Stress and Growth*, Springer-Verlag Publisher, 2nd Edition, 1990.

[Fung, 1965] - Fung Y C, *Foundation of Solid Mechanics*, Prentice Hall, 1st Edition, 1965.

[McDonalds, 1990] - O'Rourke M F and Nichols W W, *Blood Flow in Arteries,* Thomas Press, 3rd Edition, 1990.

[Rao, 1965] – Rao C R, *Linear Statistical Inference and Its Applications,* John Wiley and sons, 1965.

[Kay, 1993] – Kay S M, *Statistical Signal Processing: Estimation Theory,* Prentice Hall, 1993.

[Vonesh, Chinchilli, 1997] – Vonesh E F, Chinchilli V M, *Linear and Non linear Models for Analysis of Repeated Measurements,* Marcel Dekker, 1997.

[Trees, 2001] – Van Trees H L, *Detection Estimation and Modulation Theory – Part 1,* John Wiley, 2001.

[Beale, 1988] - Beale E M L, *Introduction to Optimization*, Wiley-Interscience Publication, 1988.

[Nelder, Mead, 1965] - Nelder J A and Mead R, *A Simplex Method for Function Minimization. Comput. J.* 7, 308-313, 1965.

[Scales, 1985] - Scales L E, *Introduction to Non-Linear Optimization*, Springer-Verlag Publication, 1985.

[Walsh, 1975] - Walsh G R, *Methods of Optimization*, Wiley- Interscience Publication, 1975.

[Coleman, Li 1996] - Coleman, T.F. and Y. Li, *An Interior, Trust Region Approach for Nonlinear Minimization Subject to Bounds,* SIAM Journal on Optimization, Vol. 6, pp. 418-445, 1996.

[Ashcraft, 2002] – Ashcraft C C, *Solving linear systems using Spooles 2.2,* Boeing Phantom Works, 2002.

[Bergel, 1961] – Bergel D H, *The static elastic properties of arterial wall,* J. Physiology, pp 445-457, 1961.

[Peskin, 2002] – Peskin C, *Immersed Boundary Method,* Cambridge University Press, 2002.

[Rosar, Peskin, 2001] – Rosar M E, Peskin C, *Fluid Flow in collapsible elastic tube: 3D Numerical Model,* New York J. Mathematics, pp 281-302, 2001.

[Hasegawa, 2006] – Hasegawa H, *Improving accuracy in estimation of arterial wall displacement by referring to center frequency of RF echo,* IEEE Trans. On Ultrasonics, vol 53.no1, January 2006.

[Whietley, 2005] – Whiteley, *Solution of inverse nonlinear elasticity problem that arise when locating breast tumors,* Francis and Taylor, J. Theoritical Medicine, vol6.no3, pp 143-149, September 2005.

[Garbey, 2005] – Garbey, *Estimation of blood flow speed and location from thermal video,* IEEE computer society conference, 2004.

[Reichek, 1999] – Reichek N, *MRI Myocardial Tagging,* J. Magnetic Resonance Imaging 10, pp 609-616, 1999.

[Gill, 1985] – Gill, *Measurement of Blood Flow by Ultrasound: Accuracy and Sources of Error,* Ultrasound in Medicine and Biology, vol 11.no 4, pp 25-641, 1985.

[Cristopher, Starkoski, 1986] - Cristopher, Starkoski, *A High Frequency pulsed wave Doppler Ultrasound for detecting and imaging blood flow,* IEEE Ultrasonics symposium, 1996.

[Whitemore, 1968] – Whitemore R L, *Theology of Circulation,* Permagon Press, 1968.

[Schmid-Schonbein, 1976] – Schmid-Schonbein H, *Microrheology of erythrocytes, blood viscosity and the distribution of blood flow in microcirculation,* International review of cardiovascular physiology, 2, vol 9, pp 1-62, University Press, 1976.

[Cokelet et al., 1980] – Cokelet G R, Meisalman H J, Brookes D E, *Erythrocyte Mechanics of Blood Flow,* New York Press, 1980.

[Dintenfass, Seaman, 1981] – Dintenfass L, Seaman G V F, *Blood Viscosity in heart diseases and cancer,* Permagon press, 1981.

[Dintenfass, 1985] – Dintenfass L, *Blood Viscosity, Hyperviscosity and hyperviscoaemia,* MTP Press, 1985.